Supplement of: An improved carbon greenhouse gas simulation in GEOS-Chem version 12.1.1

Beata Bukosa et al.

Correspondence: Beata Bukosa (beata.bukosa@niwa.co.nz)

S1 CH_4 loss via OH differences

There are 3 main differences in obtaining the $L(\mathrm{CH}_{4Trop})$ fields between the full chemistry (used by the uncoupled) and the coupled simulations (coupled and *coupled-origOH*) that could lead to the observed differences in the production of CO from CH_4. 1) In the full chemistry simulation the CH_4 values used to calculate the $L(\mathrm{CH}_{4Trop})$ are prescribed and set to fixed values, with one annual value for each of four latitude bands (30–90° S, 0–30° S, 0–30° N, 30–90° N), and throughout the troposphere. The CH_4 values are defined as averages of surface observations from NOAA carbon cycle surface flasks over the four latitudinal bands (http://wiki.seas.harvard.edu/geos-chem/index.php/Tropospheric_chemistry_mechanism#CH4_concentrations). As only one annual value is used per latitude, the seasonality of $L(\mathrm{CH}_{4Trop})$ and $P(\mathrm{CO})_{\mathrm{CH}_4}$ is only driven by OH. In our coupled simulations the CH_4 values are based on the different CH_4 emission inventories that include both CH_4 interannual and seasonal variation. Hence, the resulting CH_4 loss is not purely driven by the seasonality of the OH field, but it is also impacted by the seasonality and spatial distribution of the CH_4 sources and additional sink terms. 2) In the coupled simulations an additional soil sink is applied to the CH_4 values at the surface, that might lead to weaker CH_4 loss via OH at surface levels, since part of CH_4 is consumed by the soil sink. This sink term is not applied in the full chemistry simulation used to derive the $P(\mathrm{CO})_{\mathrm{CH}_4}$ fields for the uncoupled CO simulation. 3) OH fields from different versions of the full chem simulation (Fig. 2 and 3).

To tackle these differences we perform additional uncoupled CH_4, coupled and full chemistry simulations of the $L(\mathrm{CH}_4)$ fields. Figure S1 shows the $L(\mathrm{CH}_4)$ at the surface based on the different simulations. The red and turquoise lines represent the $L(\mathrm{CH}_4)$ from the uncoupled and *coupled-origOH* simulation. The only difference between the two simulations is that in the *coupled-origOH* there is an additional diurnal cycle added to OH. Both simulations use GEOS-Chem v5-07-08 OH fields. The indigo line represents the coupled simulation where we update the default v5-07-08 OH field to v9-01-03, the same field that is used for calculating the CO loss via OH. We use the results from this simulation to identify the impact of different OH versions on the $P(\mathrm{CO})_{\mathrm{CH}_4}$. The yellow solid line represents the $L(\mathrm{CH}_4)$ from the full chemistry simulation used to create $P(\mathrm{CO})_{\mathrm{CH}_4}$ for the uncoupled CO simulation. Although we do not have the original $L(\mathrm{CH}_4)$ fields from the full chemistry simulation, due to the 100% yield conversion between the $P(\mathrm{CO})_{\mathrm{CH}_4}$ and $L(\mathrm{CH}_{4Trop})$ these fields have the same temporal and spatial distribution. However, in regions where $P(\mathrm{CO})_{\mathrm{CH}_4}$ overestimates the total $P(\mathrm{CO})$, the $P(\mathrm{CO})_{\mathrm{CH}_4}$ fields are capped to the $P(\mathrm{CO})$ values, but, the impact of this correction on $P(\mathrm{CO})_{\mathrm{CH}_4}$ is small and mainly occurring in the tropics, in

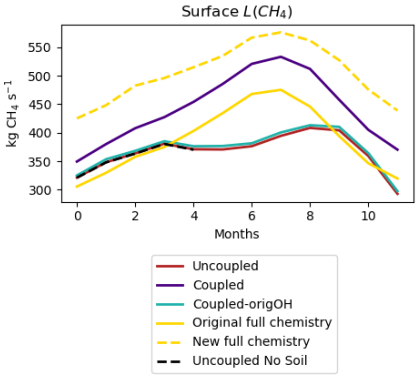

Figure S1. Surface $L(\mathrm{CH_4})$ based on different test simulations; uncoupled $\mathrm{CH_4}$ simulation (red, year 2008), coupled (indigo, year 2008), *coupled-origOH* (turquoise, year 2008), original full chemistry (yellow solid, year 2008), new full chemistry (yellow dashed, year 2008), uncoupled $\mathrm{CH_4}$ simulation without soil sink (black, year 2005, only run for January–May).

regions of deep convection. Yellow dashed line represents the $L(\mathrm{CH_4})$ from a new full chemistry simulation with GEOS-Chem version 12. The newer version of the simulation uses monthly and updated $\mathrm{CH_4}$ values in contrast to one annual value in the original simulations; hence, the seasonal variation of $L(\mathrm{CH_4})$, similar to our coupled simulation is not purely driven by the OH seasonality. The differences between the two full chemistry simulations help us identify the impact of using annual versus seasonally varying $L(\mathrm{CH_4})$ values (difference 1). There are also few additional differences between the new and original full chemistry simulation used to create the $P(\mathrm{CO})_{\mathrm{CH_4}}$ fields in the uncoupled simulation due to model updates (e.g., additional Cl sink in the newer version, updated $\mathrm{CH_4}$ values and spatial distribution); however, these difference have a minor impact on the resulting $L(\mathrm{CH_4})$. To identify the impact of an additional soil sink we ran the uncoupled $\mathrm{CH_4}$ simulation where we disabled this sink term (black dashed line).

We find that the results from both full chemistry simulations show a similar $L(\mathrm{CH_4})$ seasonal cycle at the surface, with a maximum in August, hence the missing seasonality from the $\mathrm{CH_4}$ values do not drive the changes we observe between the uncoupled and *coupled-origOH* $L(\mathrm{CH_4})$ fields (difference 1). Turning off the additional soil sink at the surface also does not resolve the differences (difference 2). We find that the differences between OH fields are responsible for the $L(\mathrm{CH_4})$ differences at surface levels. The results using OH from the v5-07-08 (red and turquoise line) full chemistry show a dip of the $L(\mathrm{CH_4})$ field between April–August; however, with the v9-01-03 OH (indigo line), the dip disappears, and $L(\mathrm{CH_4})$ has a maximum during NH summer.

Table S1. GEOS-Chem emission inventories used for both the uncoupled and coupled carbon gas simulations.

	CO_2	CH_4	CO
Fields used by both uncoupled and coupled simulations			
Anthropogenic[a]	ODIAC[b]	EDGARv4.3.2[c]	EDGARv4.2
Europe	-	-	EMEP[d]
Mexico	-	CanMex[e]	BRAVO[f]
Canada	-	CanMex[e]	CAC[g]
USA	-	GEPA[h]	NEI[i]
Asia	-	-	MIX v1.1[j]
Biomass Burning	QFEDv2[k]	QFEDv2	QFEDv2
Biofuel Burning	Yevich and Logan[l]	-	Yevich and Logan
Ocean exchange	Takahashi et al.[m]	-	-
Balanced Biosphere	SIB3[n]	-	-
Net Terrestrial Exchange	TransCom[o]	-	-
Shipping	ICOADS[p]	-	ICOADS
Aviation	AEIC[q]	-	AEIC
Soil and Termites	-	Fung et al.[r]	-
Wetland	-	JPL WetCHARTs v1.0[s]	-
Seeps	-	Maasakkers et al. in prep.	-
Rice	-	EDGARv4.3.2	-
Cl sink	-	Maasakkers et al. (2019)	-

[a] The anthropogenic emissions in the CO simulation had regional overwrites for the countries specified in the table.
[b] Open-source Data Inventory of Anthropogenic CO_2 (Oda and Maksyutov, 2011) [c] European Commission. Emission Database for Global Atmospheric Research (http://edgar.jrc.ec.europa.eu/) [d] European Monitoring and Evaluation Programme (Vestreng et al., 2007) [e] Sheng et al. (2017) [f] The Big Bend Regional Aerosol and Visibility Observational Study (Kuhns et al., 2005) [g] Criteria Air Contaminants Van Donkelaar et al. (2012) [f] National Emissions Inventory (http://www.epa.gov/ttnchie1/net/2005inventory.html) [i] Maasakkers et al. (2016) [j] Li et al. (2017) [k] The Quick Fire Emissions Dataset (Darmenov and da Silva, 2015) [l] Yevich and Logan (2003) [m] Takahashi et al. (2009) [n] The Simple Biosphere (Messerschmidt et al., 2013) [o] Baker et al. (2006) [p] International Comprehensive Ocean–Atmosphere Data Set (Lee et al., 2011) [q] Aviation Emissions Inventory Code (Stettler et al., 2011) [r] Fung et al. (1991) [s] Bloom et al. (2017)

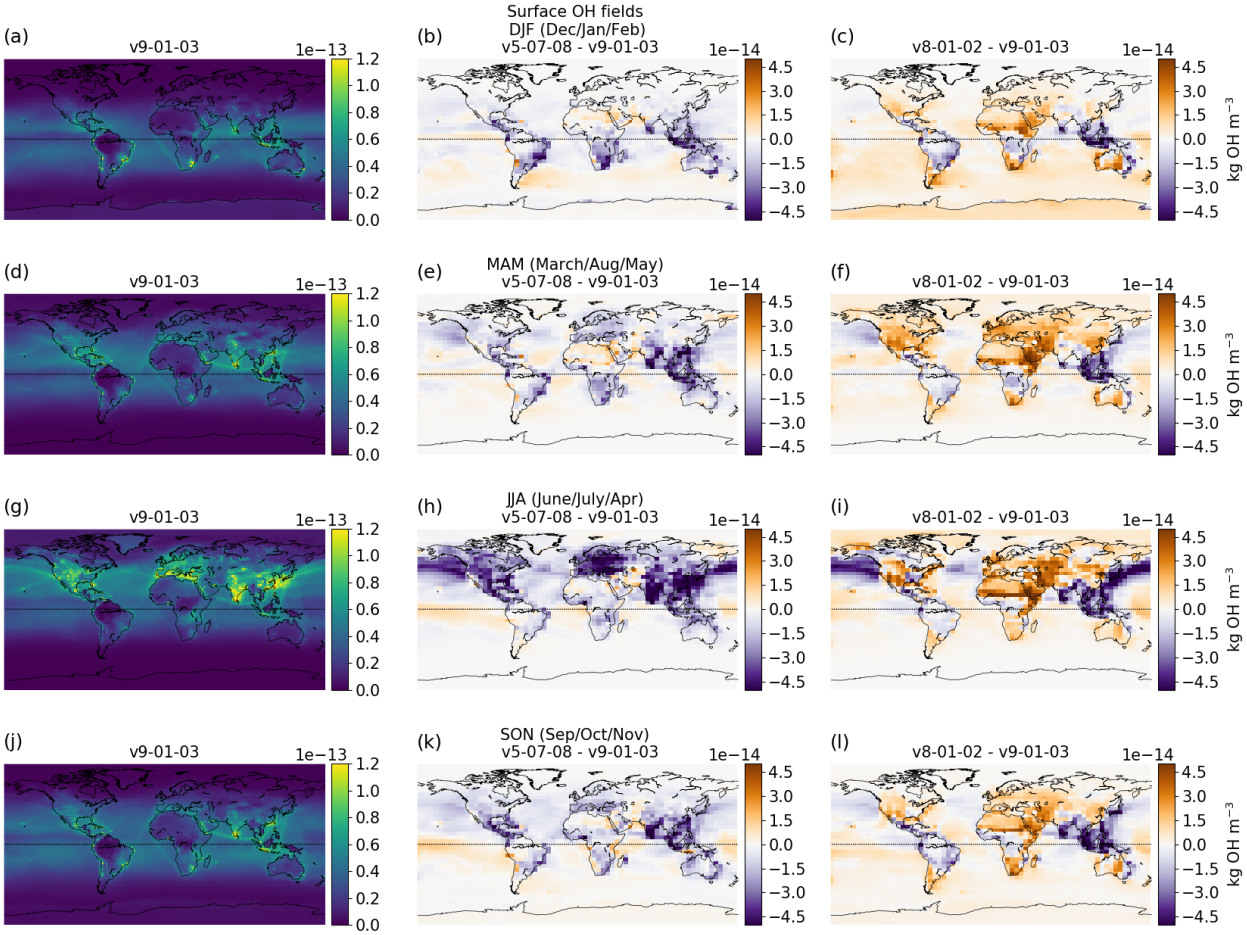

Figure S2. Surface yearly averaged global spatial distribution of the OH fields based on the v9-01-03 (a, d, g, j) full chemistry simulation and the difference between v5-07-08 - v9-01-03 (b, e, h, k) and v8-02-01 - v9-01-03 (c, f, i, l) for each season (DJF a–c, MAM d–f, JJA g–i, SON j–l).

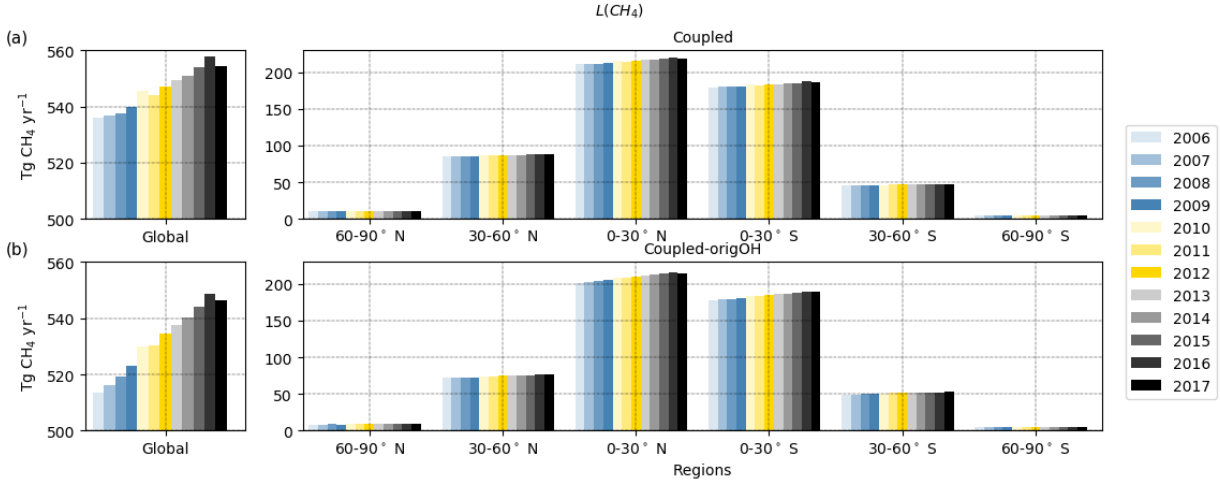

Figure S3. Annual budgets of the global and regional CH_4 loss from the coupled (a) and *coupled-origOH* (b) simulations.

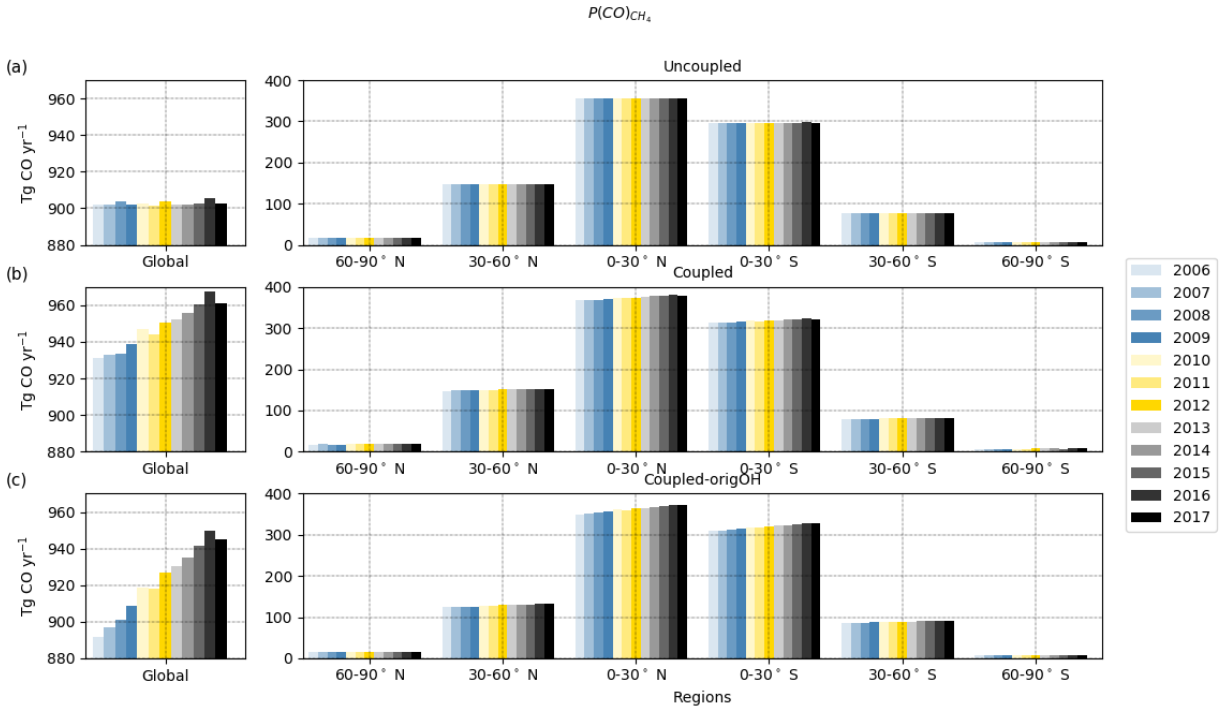

Figure S4. Annual budgets of the global and regional CO production from CH_4 from the uncoupled (a), coupled (b) and *coupled-origOH* (c) simulations.

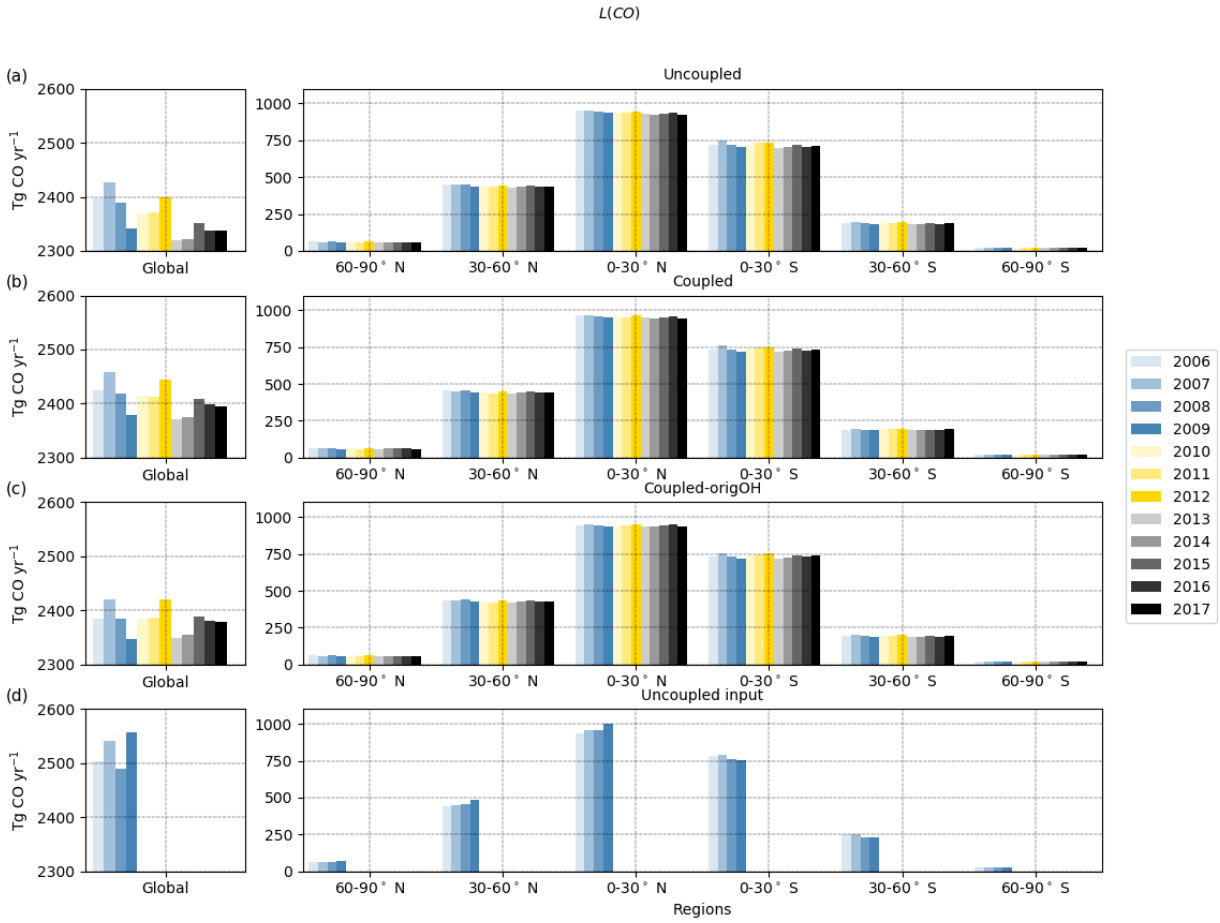

Figure S5. Annual budgets of the global and regional CO loss from the uncoupled (a), coupled (b), *coupled-origOH* (c) simulations and the input fields for the uncoupled CO_2 simulation (d).

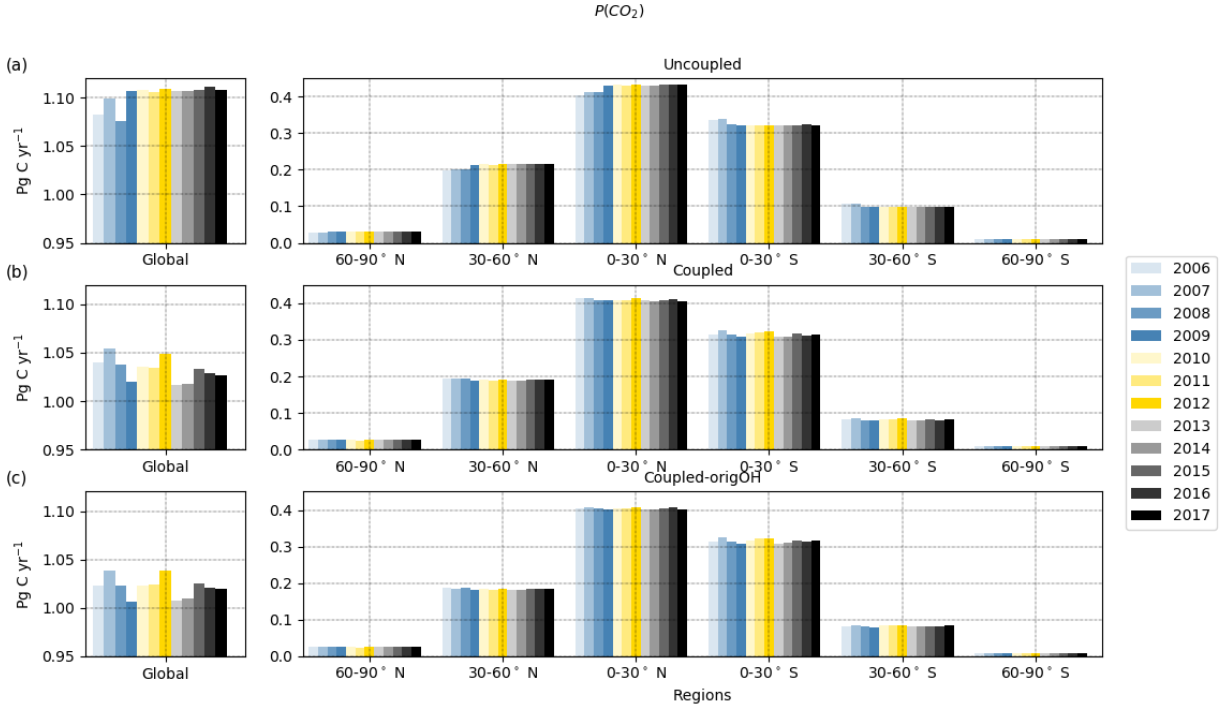

Figure S6. Annual budgets of the global and regional CO_2 production from the uncoupled (a), coupled (b) and *coupled-origOH* (c) simulations.

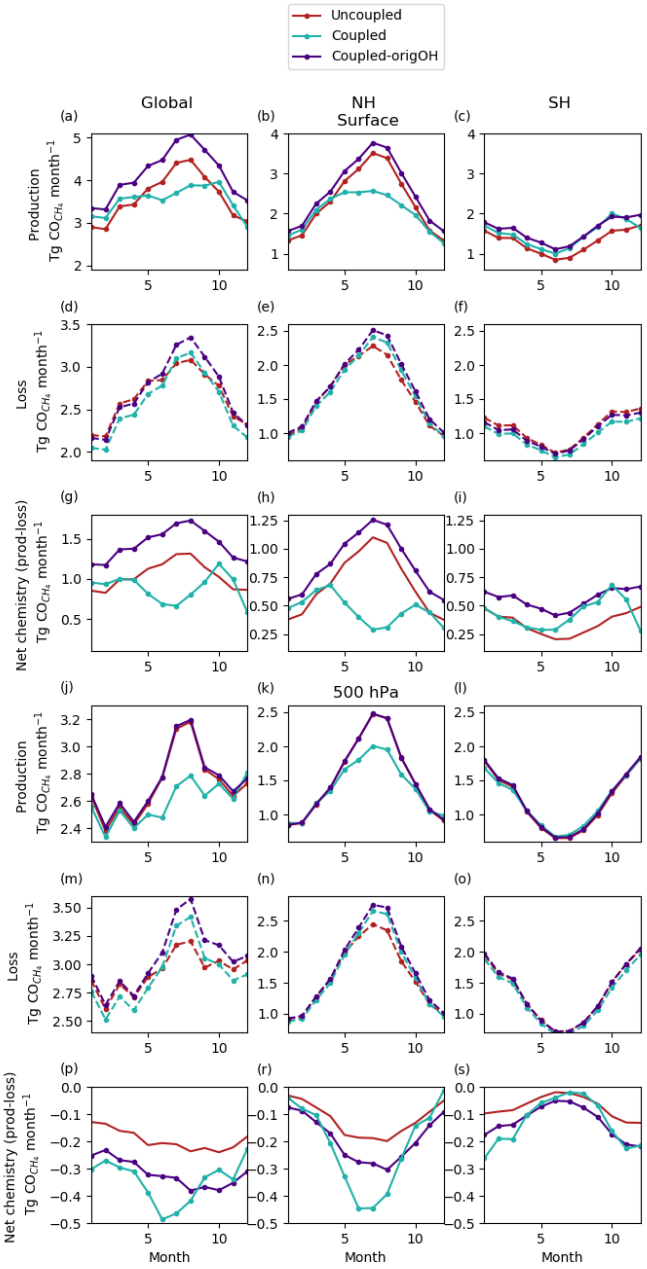

Figure S7. Global (a, d, g, j, m, p), Northern Hemisphere (b, e, h, k, n, r) and Southern Hemisphere (c, f, i, l, o, s) production of CO from CH_4 (a–c, j–l), its loss via OH (d–f, m–o) and their difference (g–i, p–s) in the uncoupled (red), coupled (indigo) and *coupled-origOH* (turquoise) simulations at the surface (a–i) and 500 hPa altitude (j–s), averaged for 2006-2017.

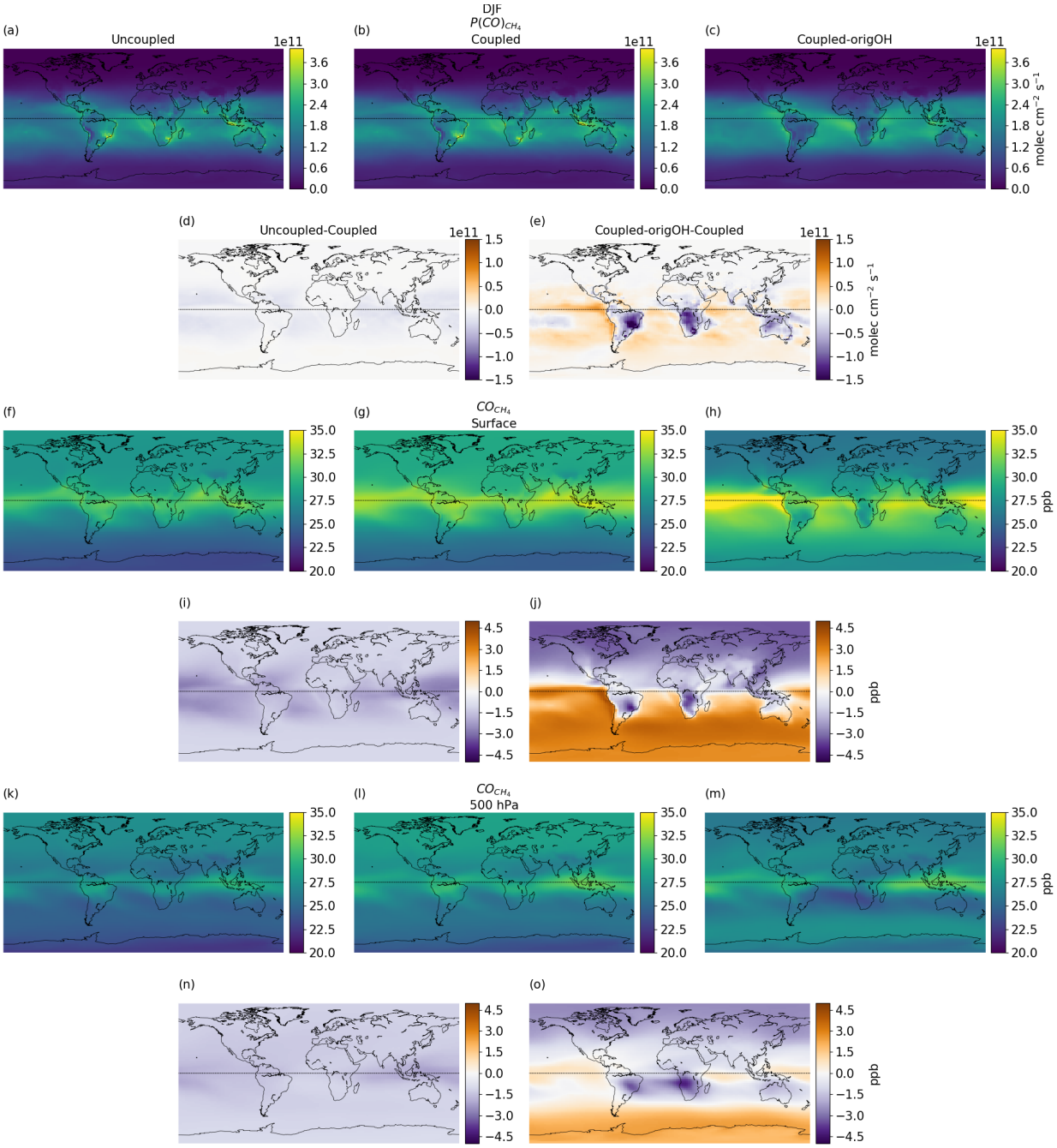

Figure S8. Average December–January–February 2006–2017 total column CO chemical production from CH_4 (a–e), corresponding mole fractions (i.e., CO_{CH_4}) at the surface (f–j) and at 500 hPa (k–o) based on the uncoupled (a, f, k), coupled (b, g, l) and *coupled-origOH* (c, h, m) simulations, and their difference relative to the coupled simulation (d, e, i, j, n, o).

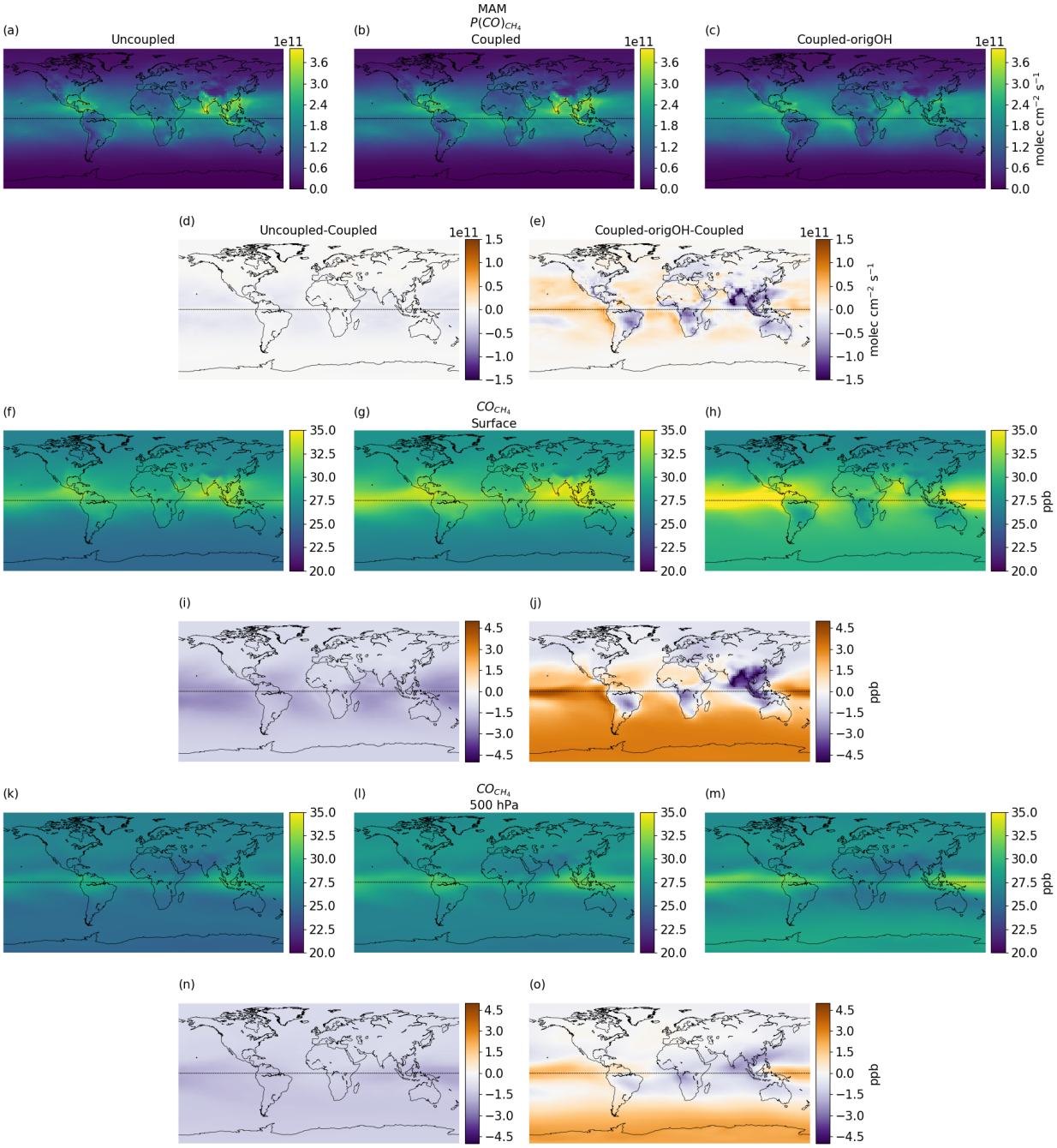

Figure S9. Average March–April–May 2006–2017 total column CO chemical production from CH_4 (a–e), corresponding mole fractions (i.e., CO_{CH_4}) at the surface (f–j) and at 500 hPa (k–o) based on the uncoupled (a, f, k), coupled (b, g, l) and *coupled-origOH* (c, h, m) simulations, and their difference relative to the coupled simulation (d, e, i, j, n, o).

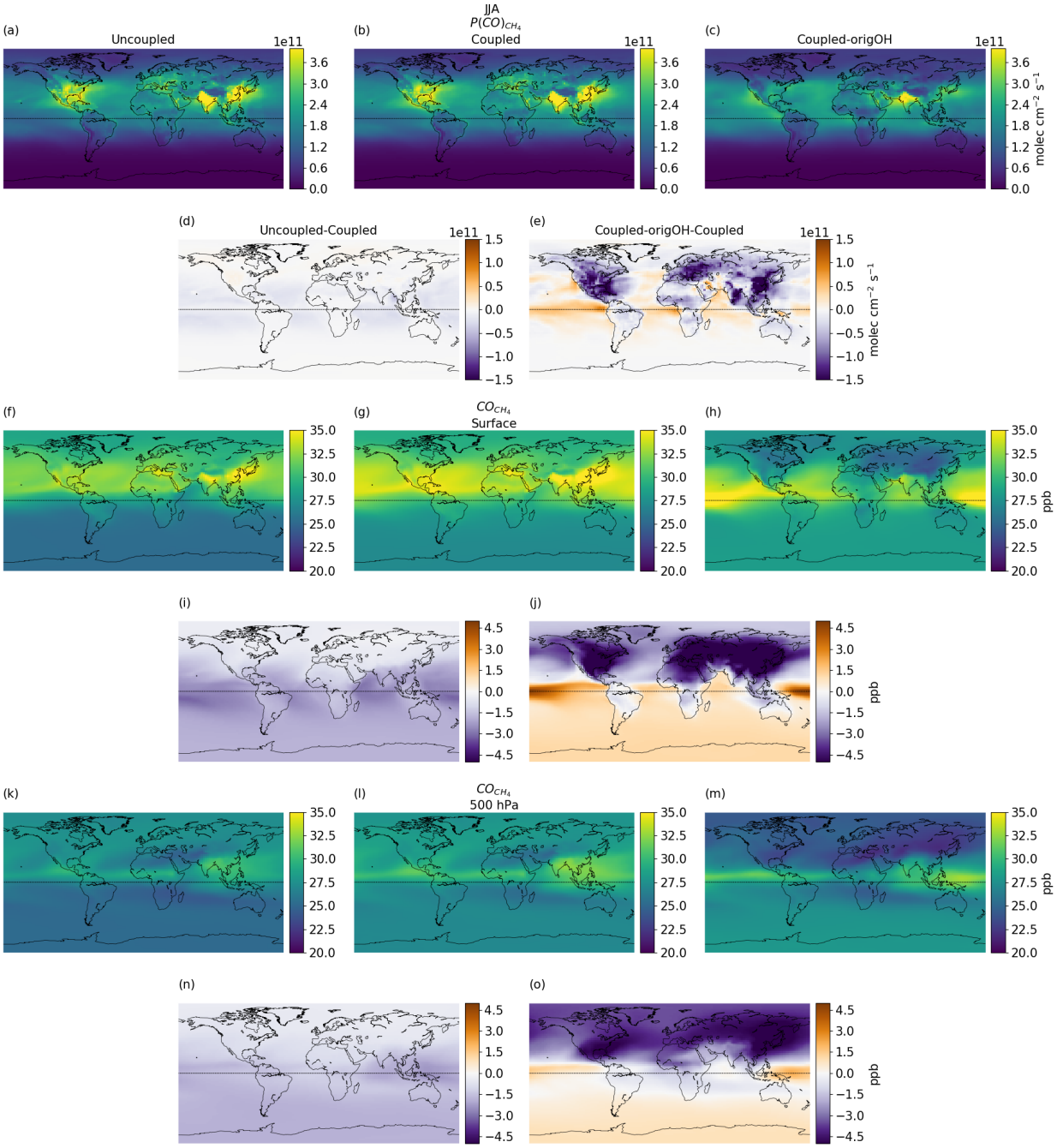

Figure S10. Average June–July–August 2006–2017 total column CO chemical production from CH_4 (a–e), corresponding mole fractions (i.e., CO_{CH_4}) at the surface (f–j) and at 500 hPa (k–o) based on the uncoupled (a, f, k), coupled (b, g, l) and *coupled-origOH* (c, h, m) simulations, and their difference relative to the coupled simulation (d, e, i, j, n, o).

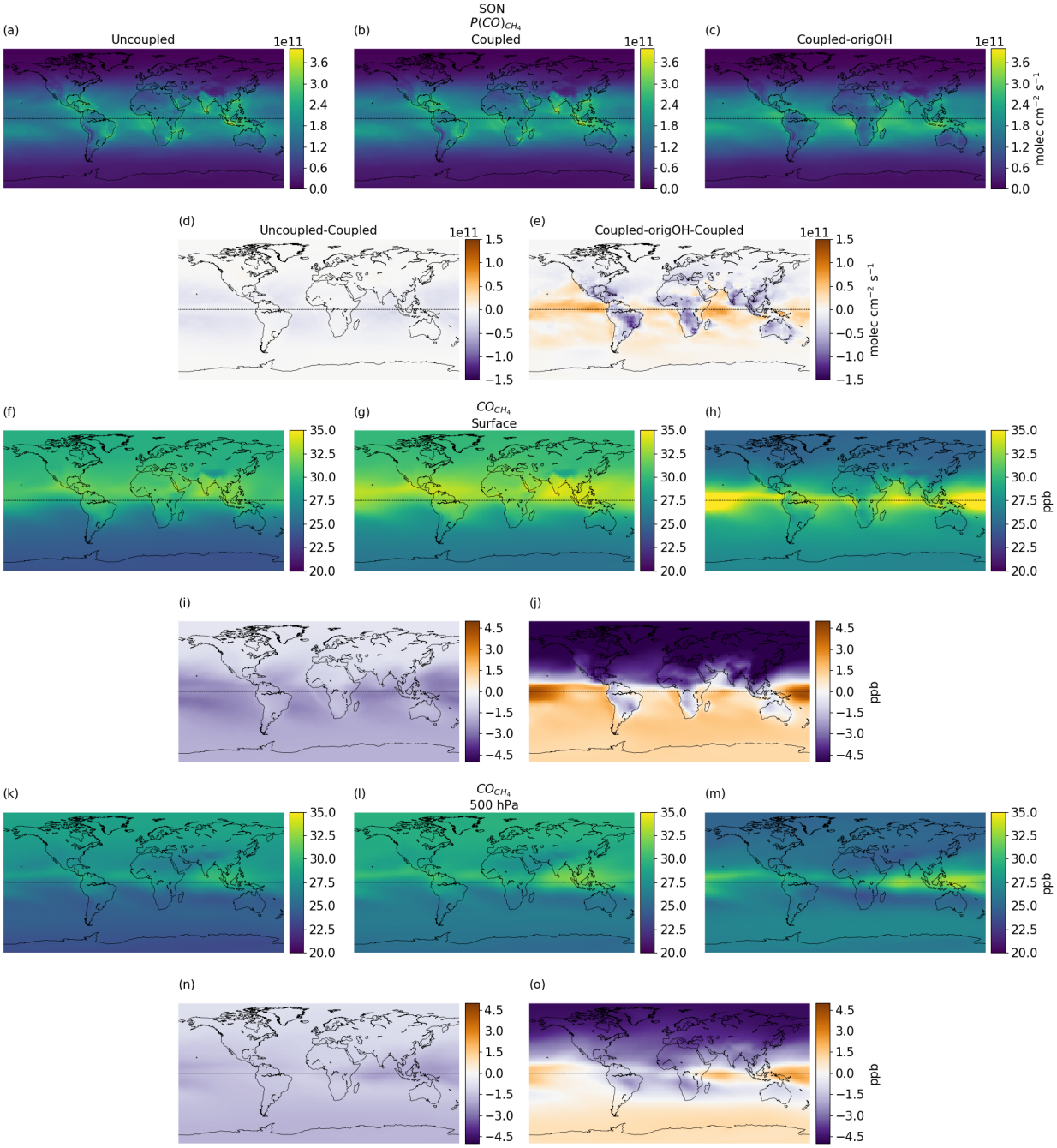

Figure S11. Average September–October–November 2006–2017 total column CO chemical production from CH_4 (a–e), corresponding mole fractions (i.e., CO_{CH_4}) at the surface (f–j) and at 500 hPa (k–o) based on the uncoupled (a, f, k), coupled (b, g, l) and *coupled-origOH* (c, h, m) simulations, and their difference relative to the coupled simulation (d, e, i, j, n, o).

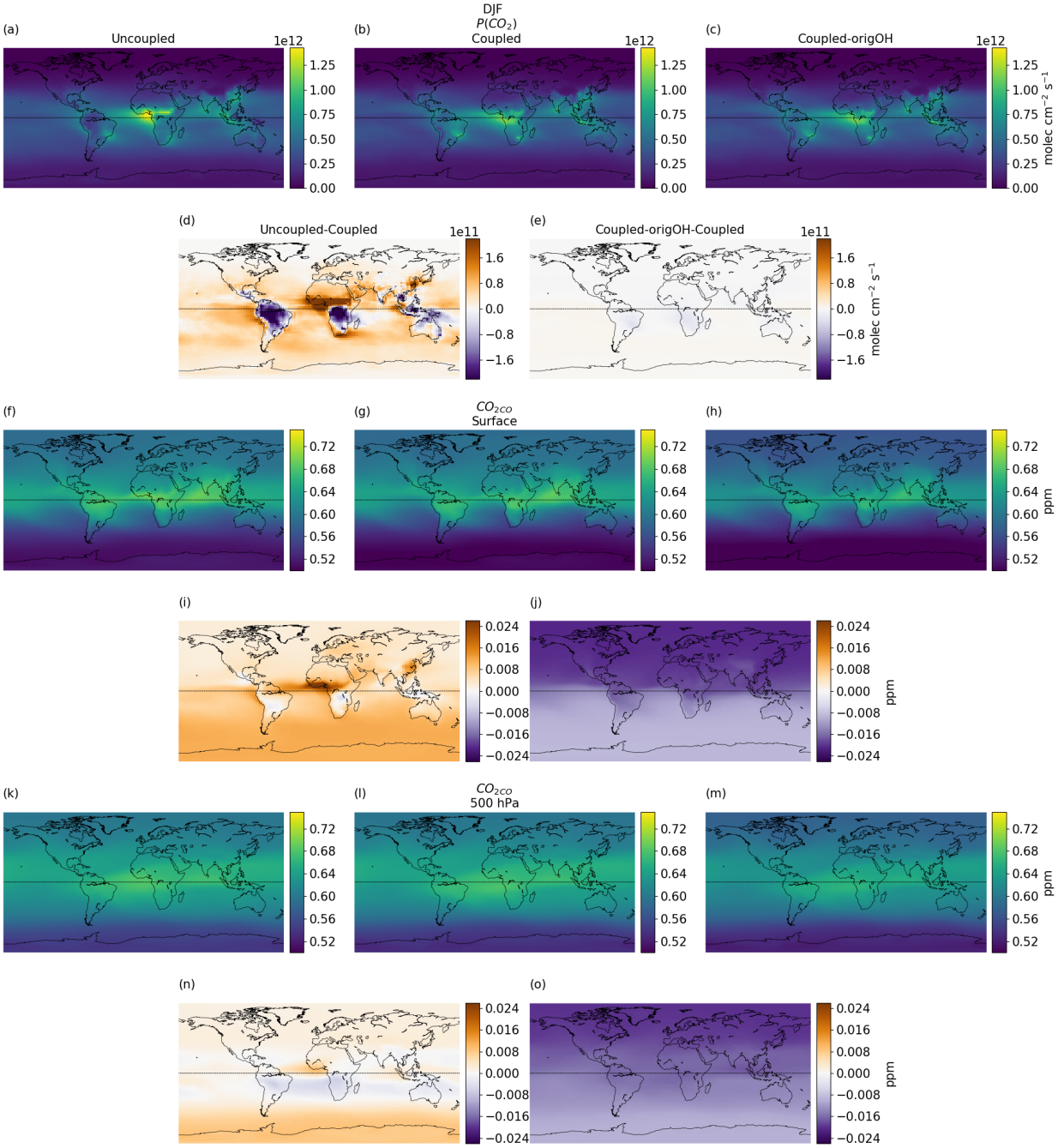

Figure S12. Average December–January–February 2006–2017 total column CO_2 chemical production from CO (a–e), corresponding mole fractions (i.e., CO_{2CO}) at the surface (f–j) and at 500 hPa (k–o) based on the uncoupled (a, f, k), coupled (b, g, l) and *coupled-origOH* (c, h, m) simulations, and their difference relative to the coupled simulation (d, e, i, j, n, o).

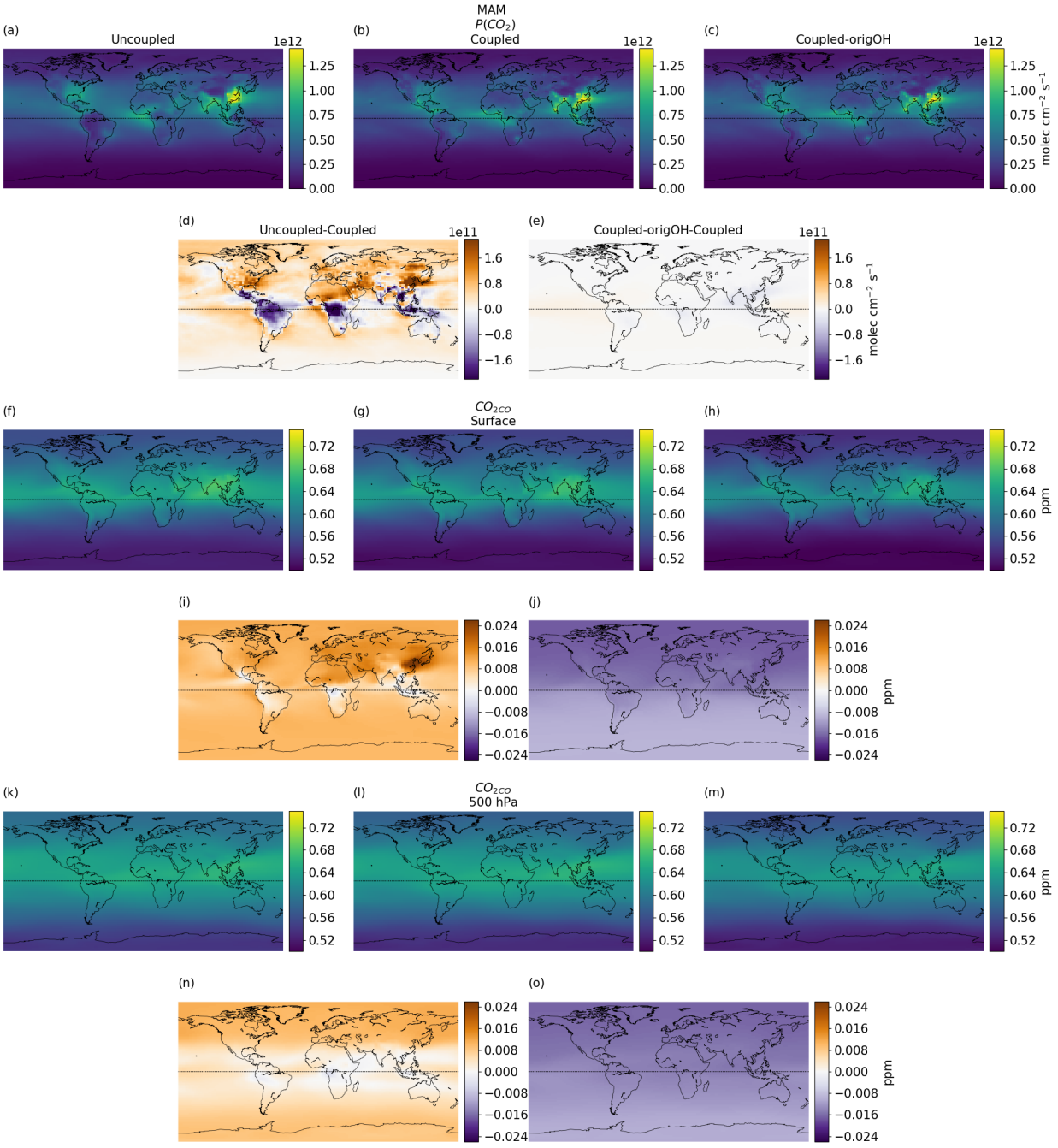

Figure S13. Average March–April–May 2006–2017 total column CO_2 chemical production from CO (a–e), corresponding mole fractions (i.e., CO_{2CO}) at the surface (f–j) and at 500 hPa (k–o) based on the uncoupled (a, f, k), coupled (b, g, l) and *coupled-origOH* (c, h, m) simulations, and their difference relative to the coupled simulation (d, e, i, j, n, o).

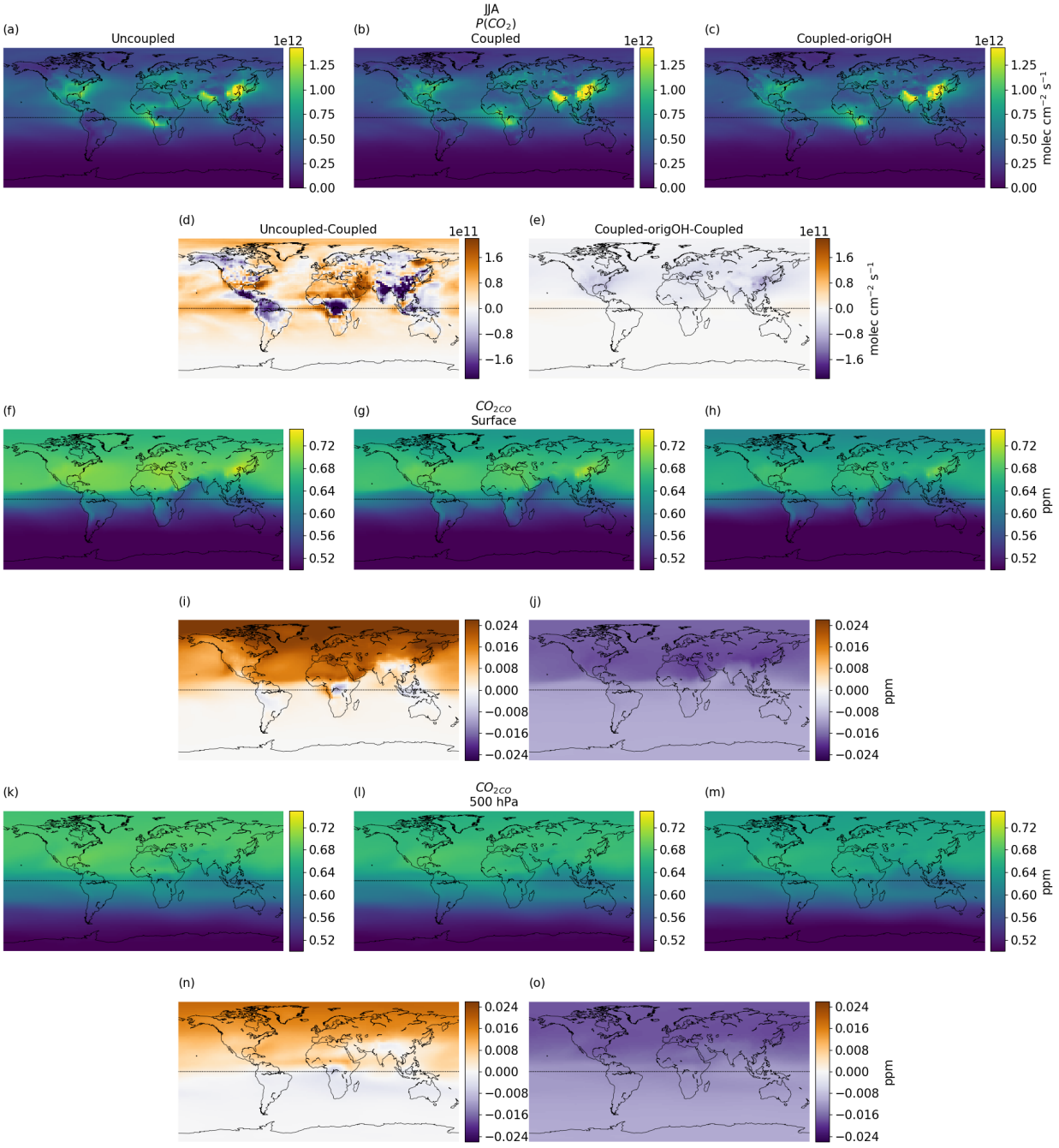

Figure S14. Average June–July–August 2006–2017 total column CO_2 chemical production from CO (a–e), corresponding mole fractions (i.e., CO_{2CO}) at the surface (f–j) and at 500 hPa (k–o) based on the uncoupled (a, f, k), coupled (b, g, l) and *coupled-origOH* (c, h, m) simulations, and their difference relative to the coupled simulation (d, e, i, j, n, o).

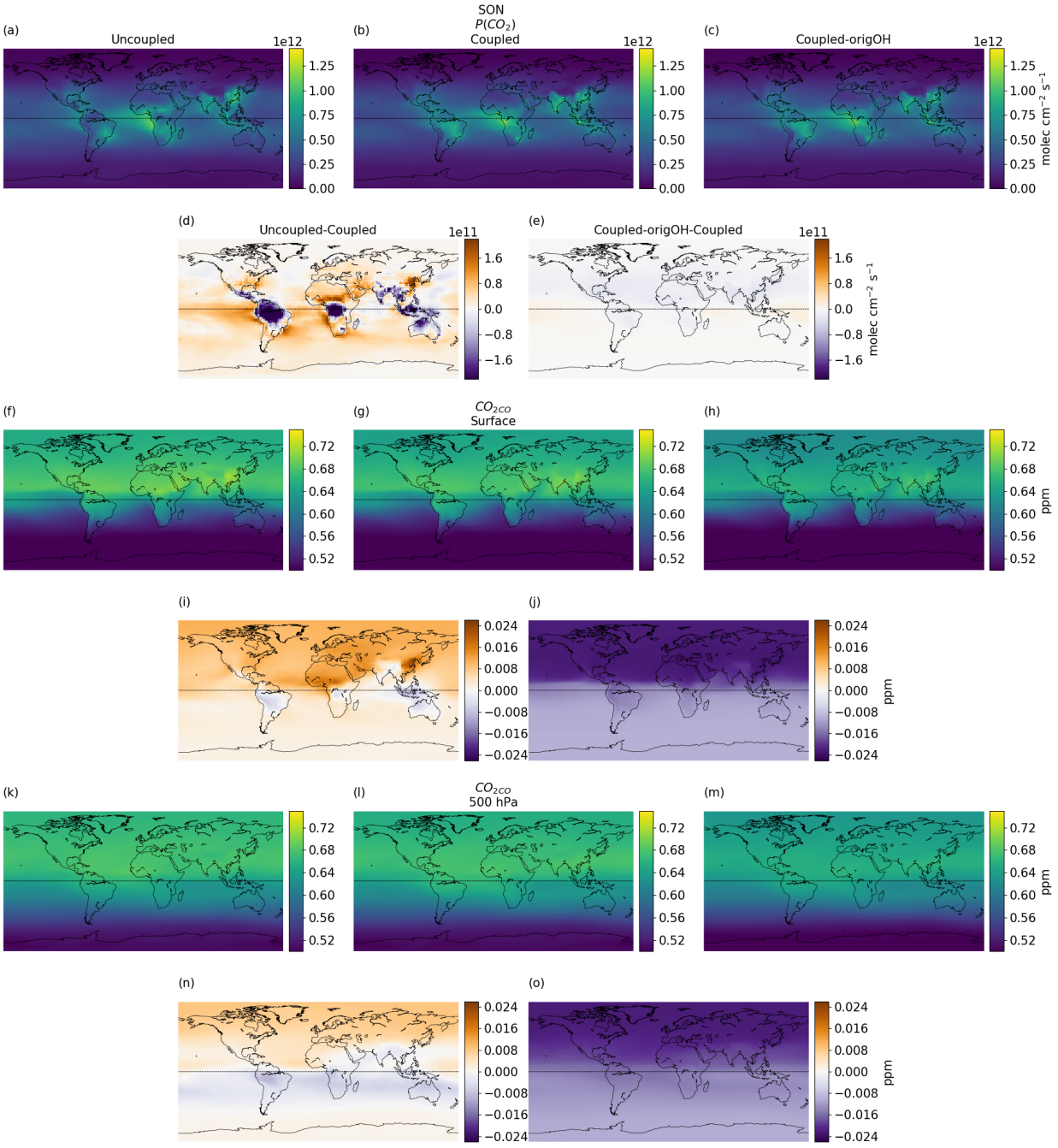

Figure S15. Average September–October–November 2006–2017 total column CO_2 chemical production from CO (a–e), corresponding mole fractions (i.e., CO_{2CO}) at the surface (f–j) and at 500 hPa (k–o) based on the uncoupled (a, f, k), coupled (b, g, l) and *coupled-origOH* (c, h, m) simulations, and their difference relative to the coupled simulation (d, e, i, j, n, o).

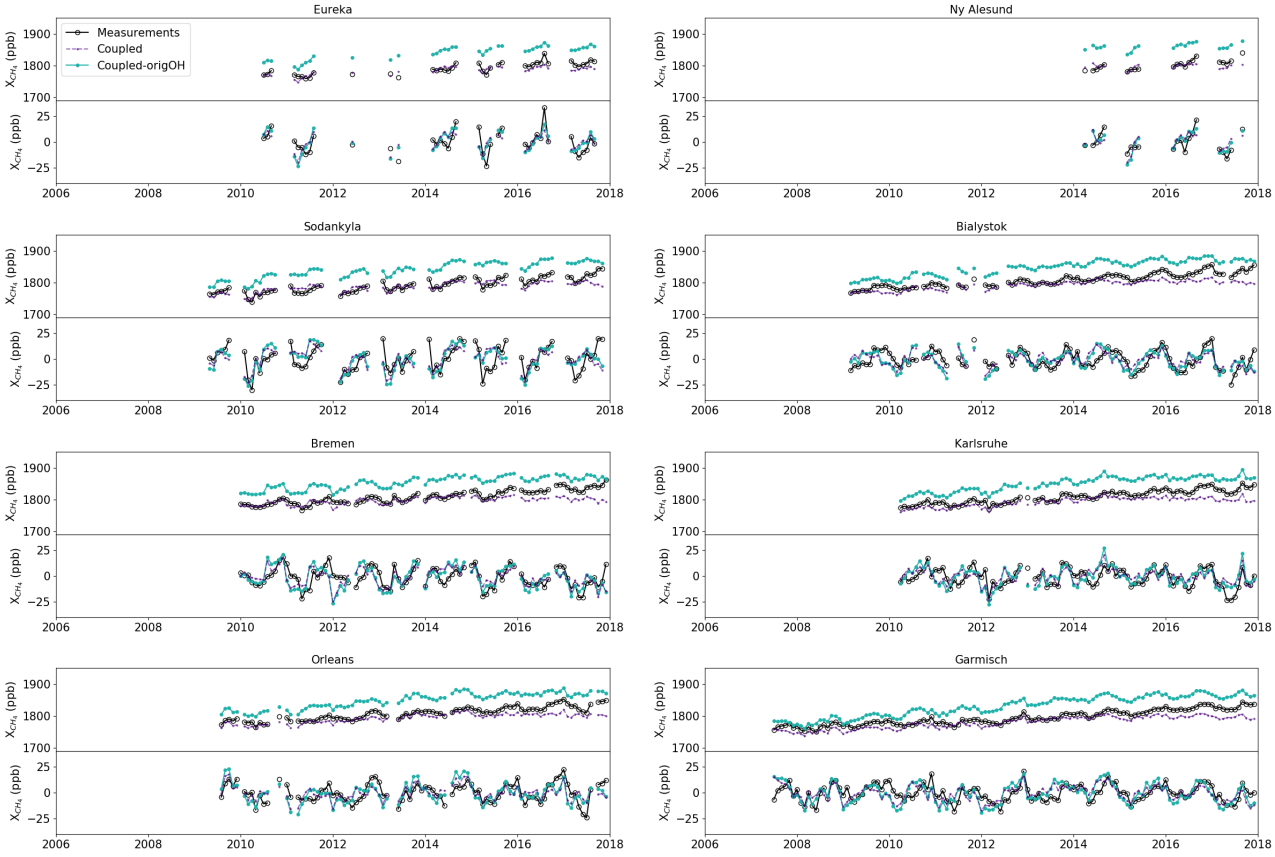

Figure S16. Modelled CH_4 (indigo-coupled, turquoise-*coupled-origOH*) comparison with column measurements (black) at different TCCON sites (top plots), based on monthly average values. The detrended values are shown in the bottom plots.

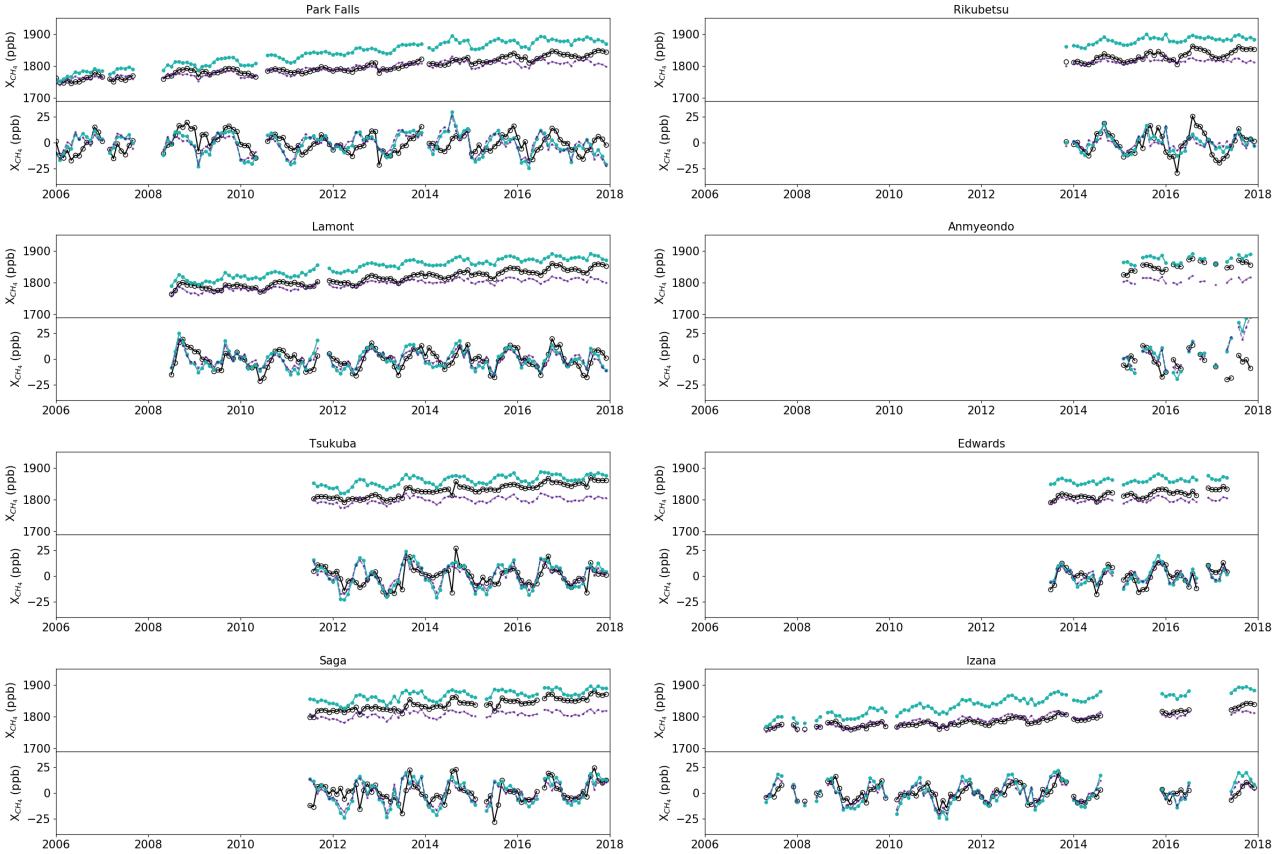

Figure S16. Continued.

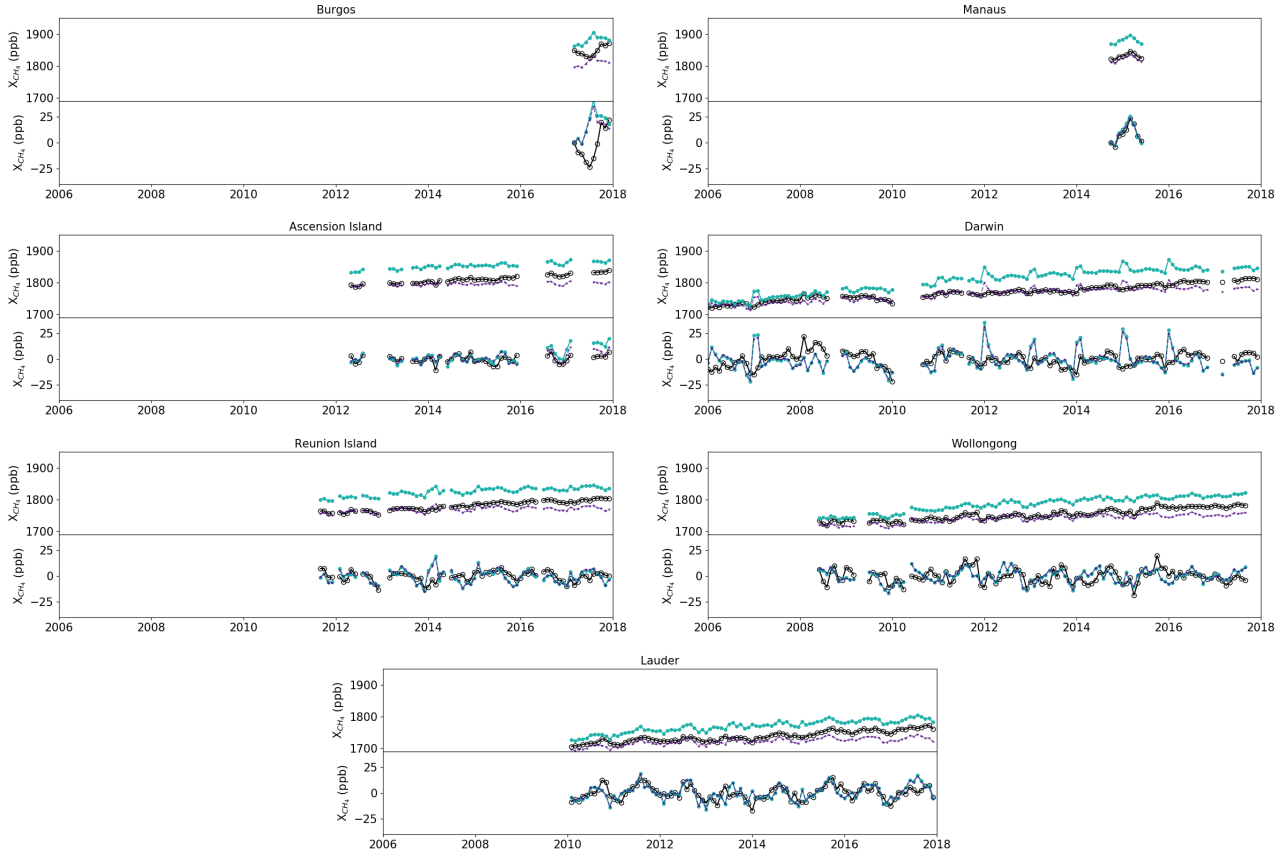

Figure S16. Continued.

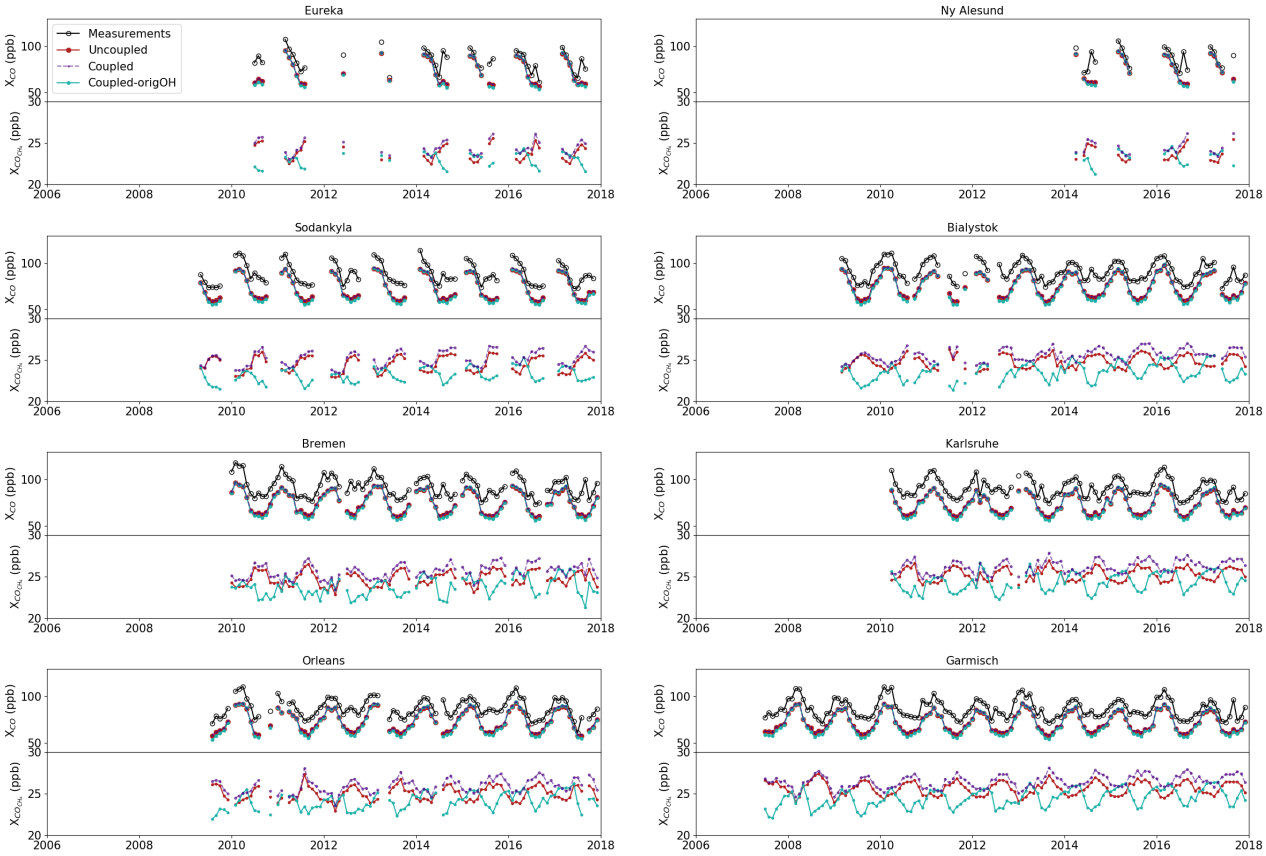

Figure S17. Modelled CO (red-uncoupled, indigo-coupled, turquoise-*coupled-origOH*) comparison with column measurements (black) at different TCCON sites (top plots), based on monthly average values. Note, the plots show the scaled CO TCCON values (see main text for details). The bottom plots represent the mixing ratios of the CO production from CH_4 from the different simulations. Note, eq. 11 cannot be directly used when calculating the column averaged dry-air mole fractions of the chemical terms (i.e., CO_{2CO} and CO_{CH_4}) since the a priori (x_a) represents the profile of the total amount of each gas and has no information about the individual source contributions. The contribution of the a priori profiles is excluded for the calculation of CO_{CH_4}, which is converted to column averaged dry-air mole fractions according to $c_s = h^T a^T x_m$.

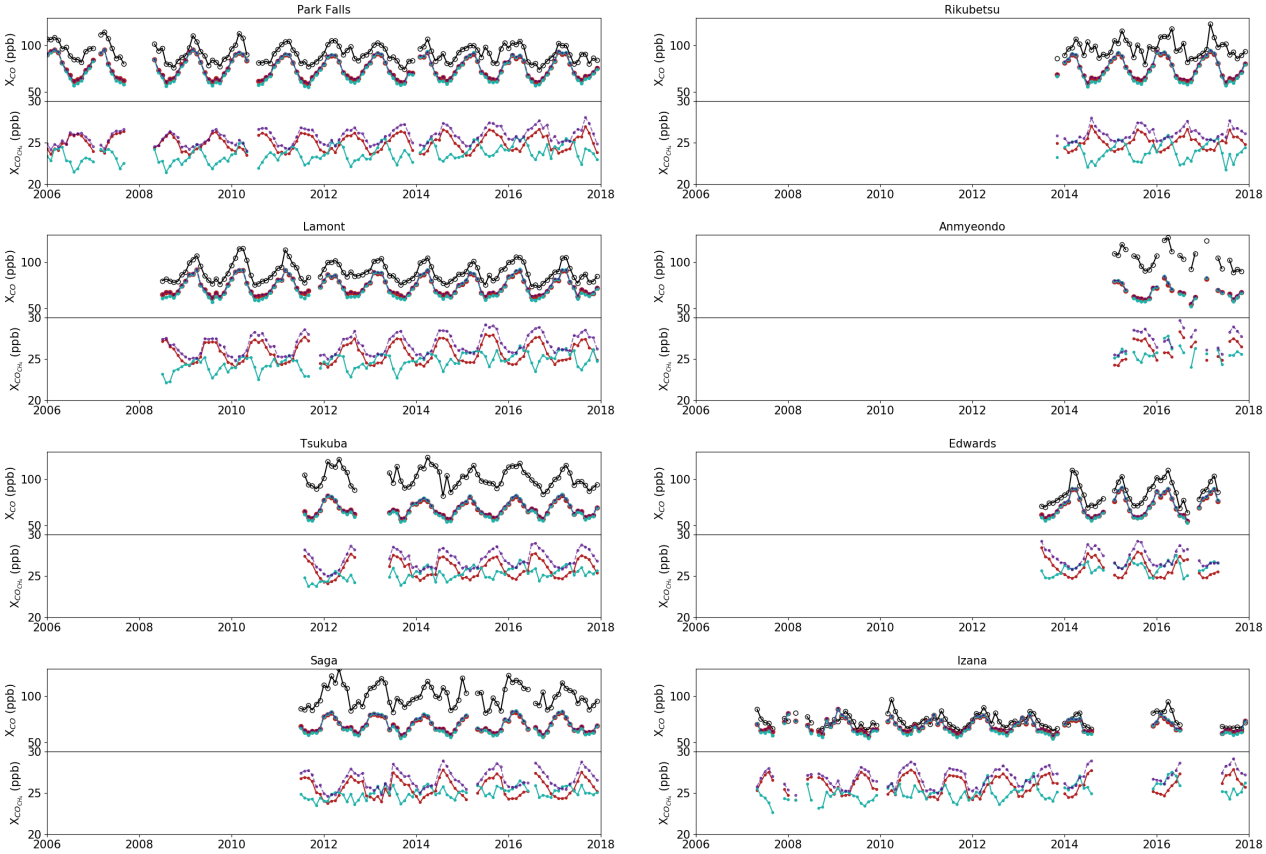

Figure S17. Continued.

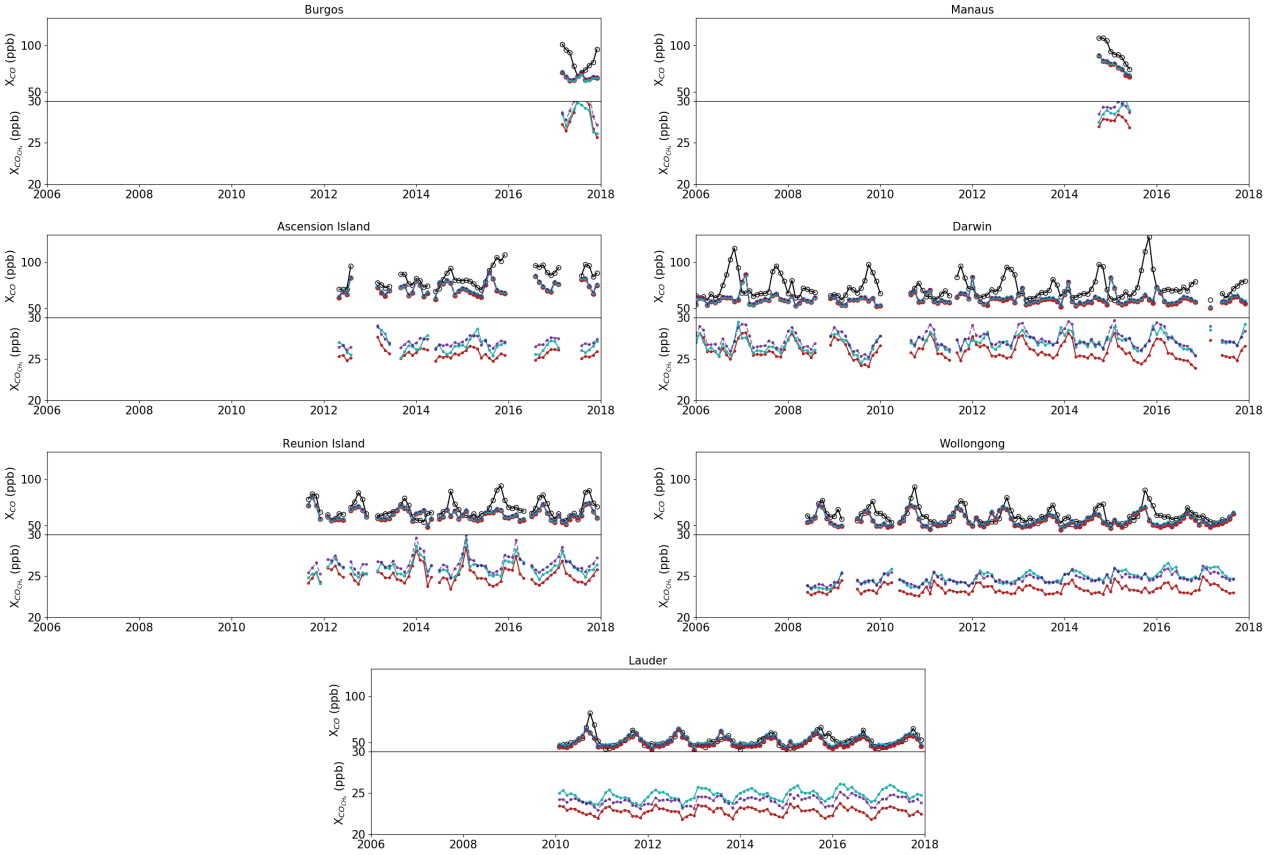

Figure S17. Continued.

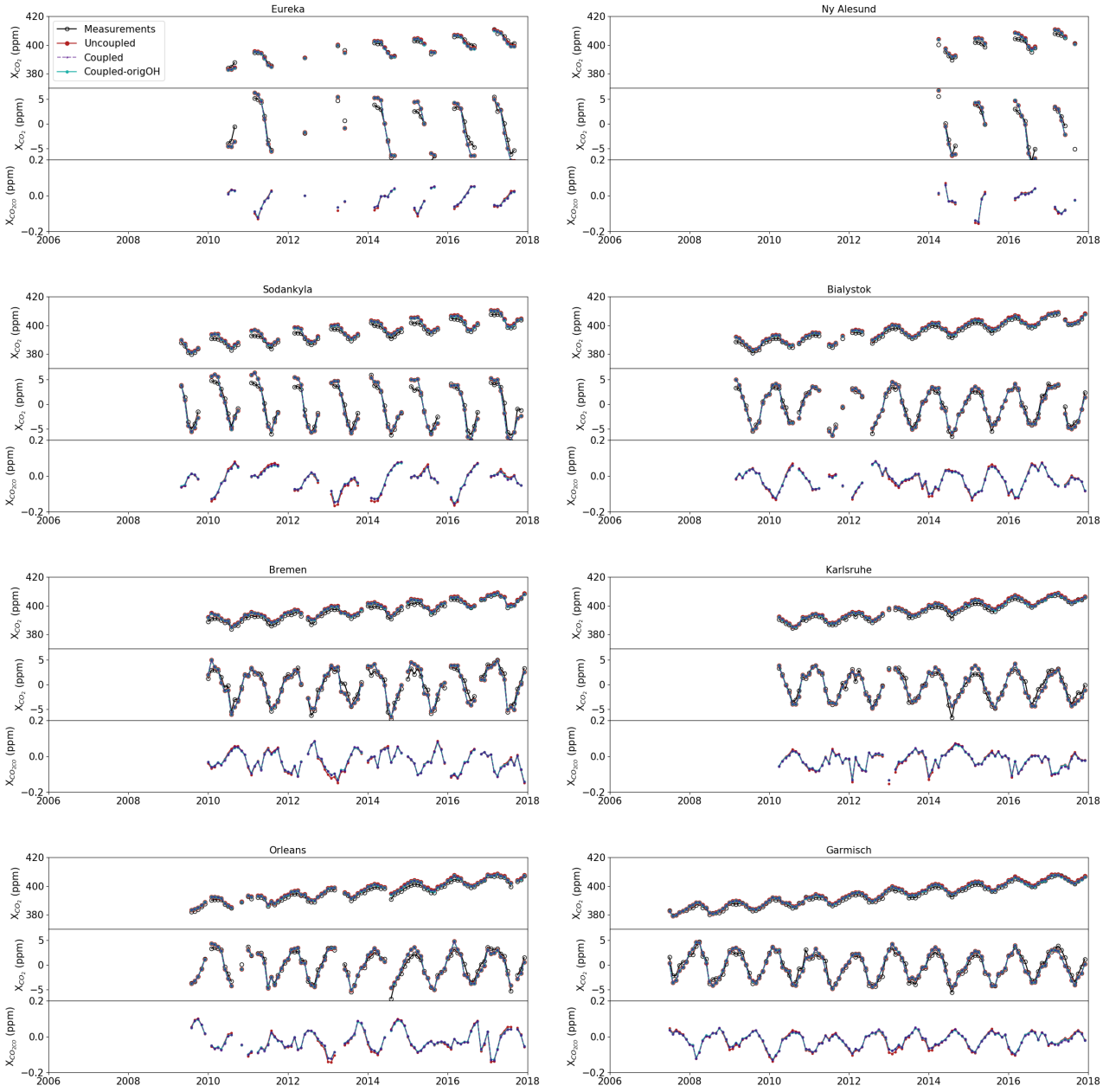

Figure S18. Modelled CO_2 (red-uncoupled, indigo-coupled, turquoise-*coupled-origOH*) comparison with column measurements (black) at different TCCON sites (top plots), based on monthly average values. The detrended values are shown in the middle plots. The bottom plots represent the detrended mixing ratios of the CO_2 production from CO from the different simulations. Note, eq. 11 cannot be directly used when calculating the column averaged dry-air mole fractions of the chemical terms (i.e., $CO_{2_{CO}}$ and CO_{CH_4}) since the a priori (x_a) represents the profile of the total amount of each gas and has no information about the individual source contributions. The contribution of the a priori profiles is excluded for the calculation of $CO_{2_{CO}}$, which is converted to column averaged dry-air mole fractions according to $c_s = h^T a^T x_m$.

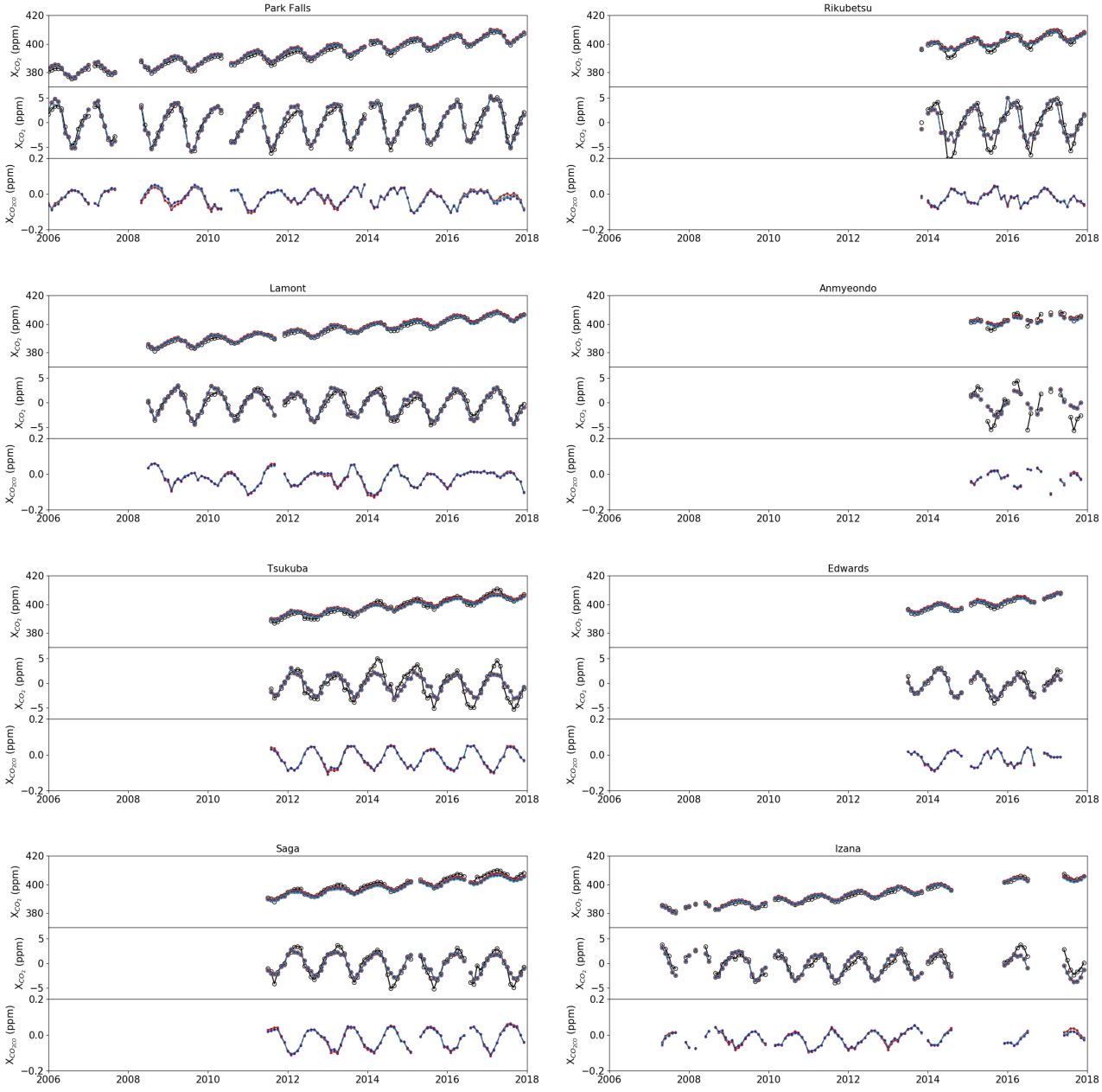

Figure S18. Continued.

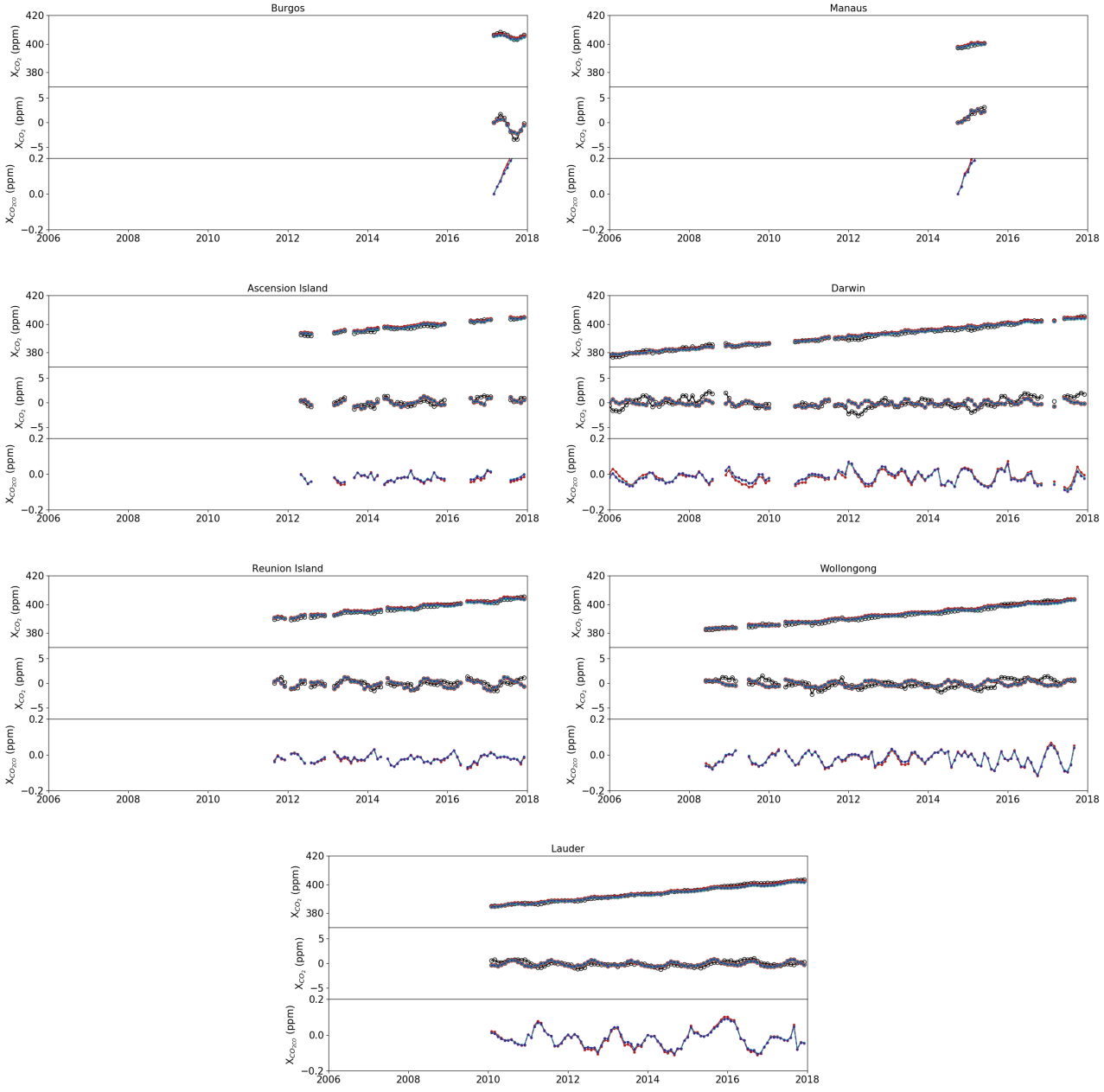

Figure S18. Continued.

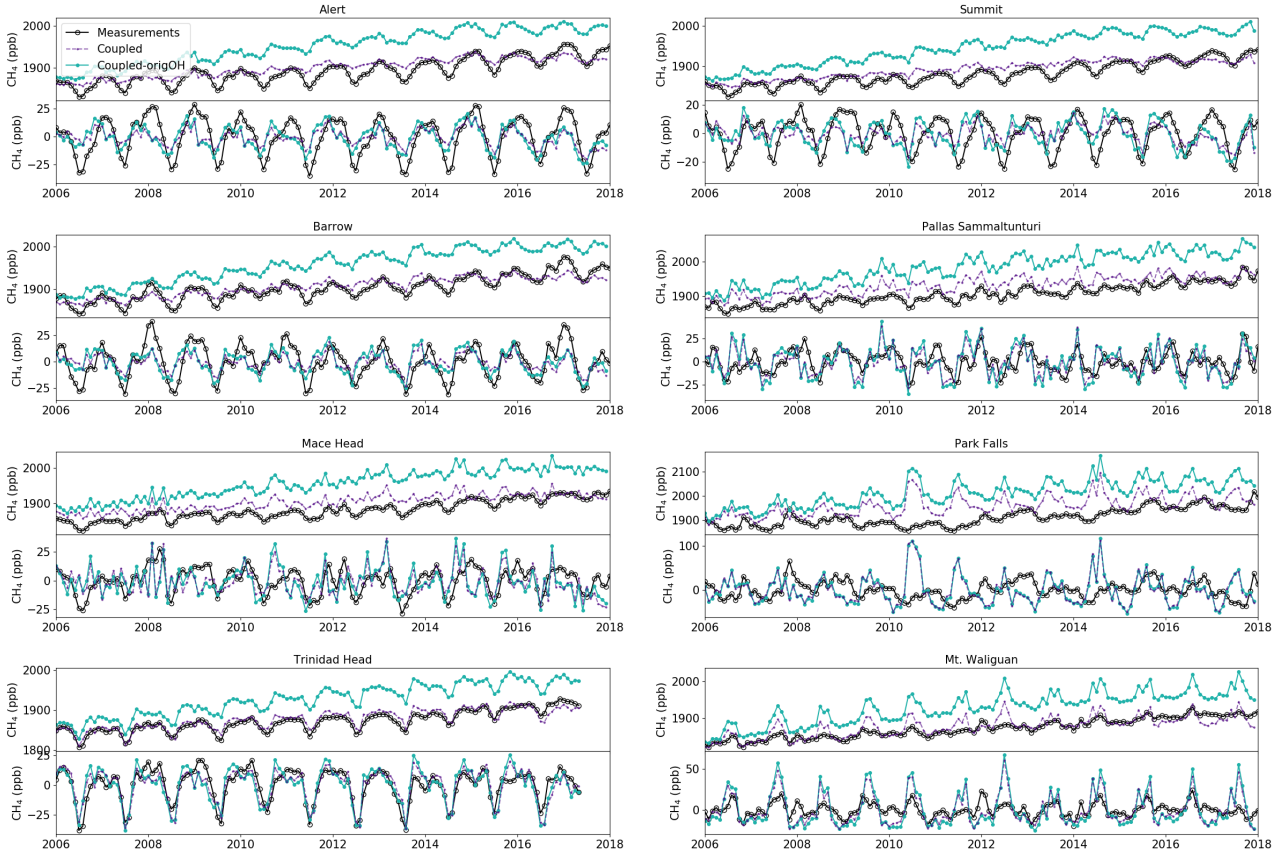

Figure S19. Modelled CH_4 (indigo-coupled, turquoise-*coupled-origOH*) comparison with surface measurements (black, top plots), based on monthly average values. The detrended values are shown in the bottom plots.

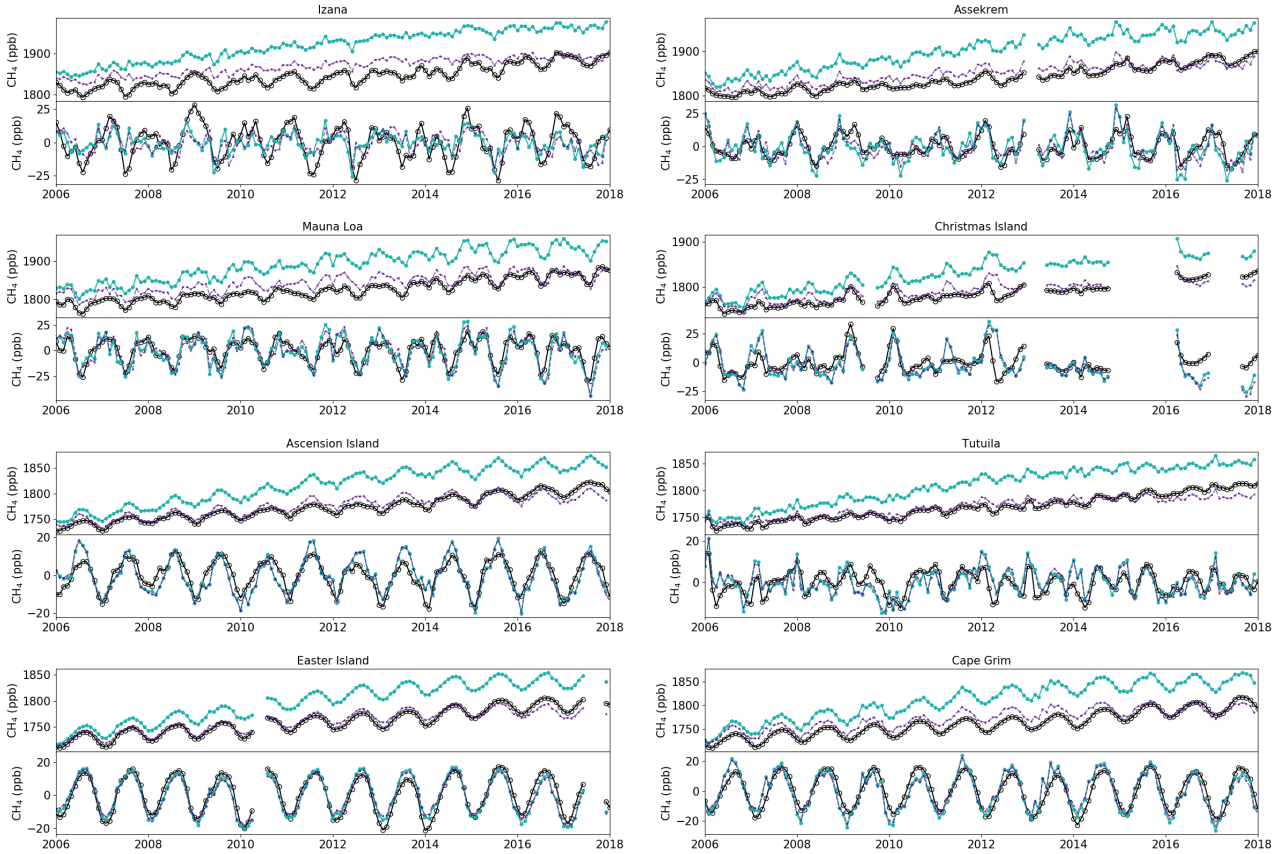

Figure S19. Continued.

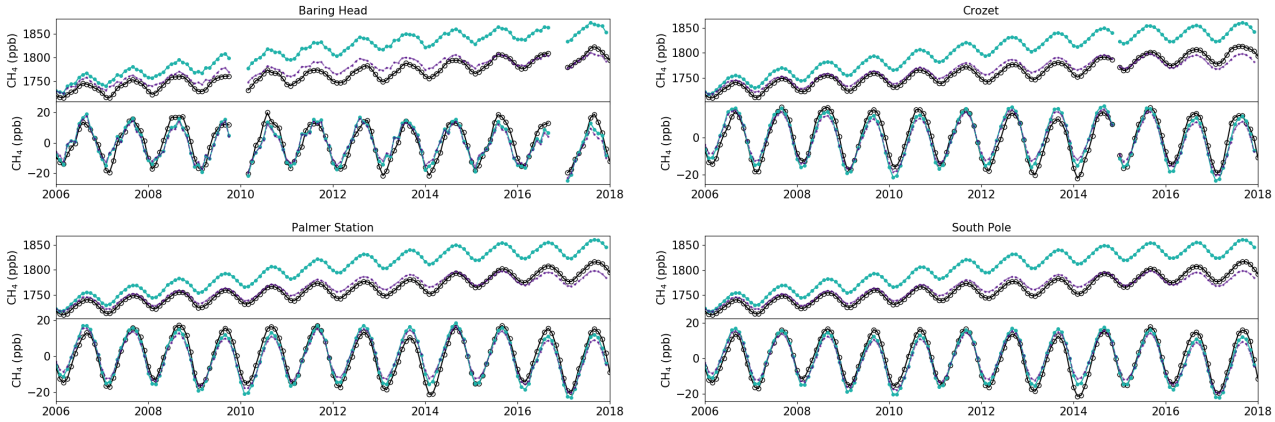

Figure S19. Continued.

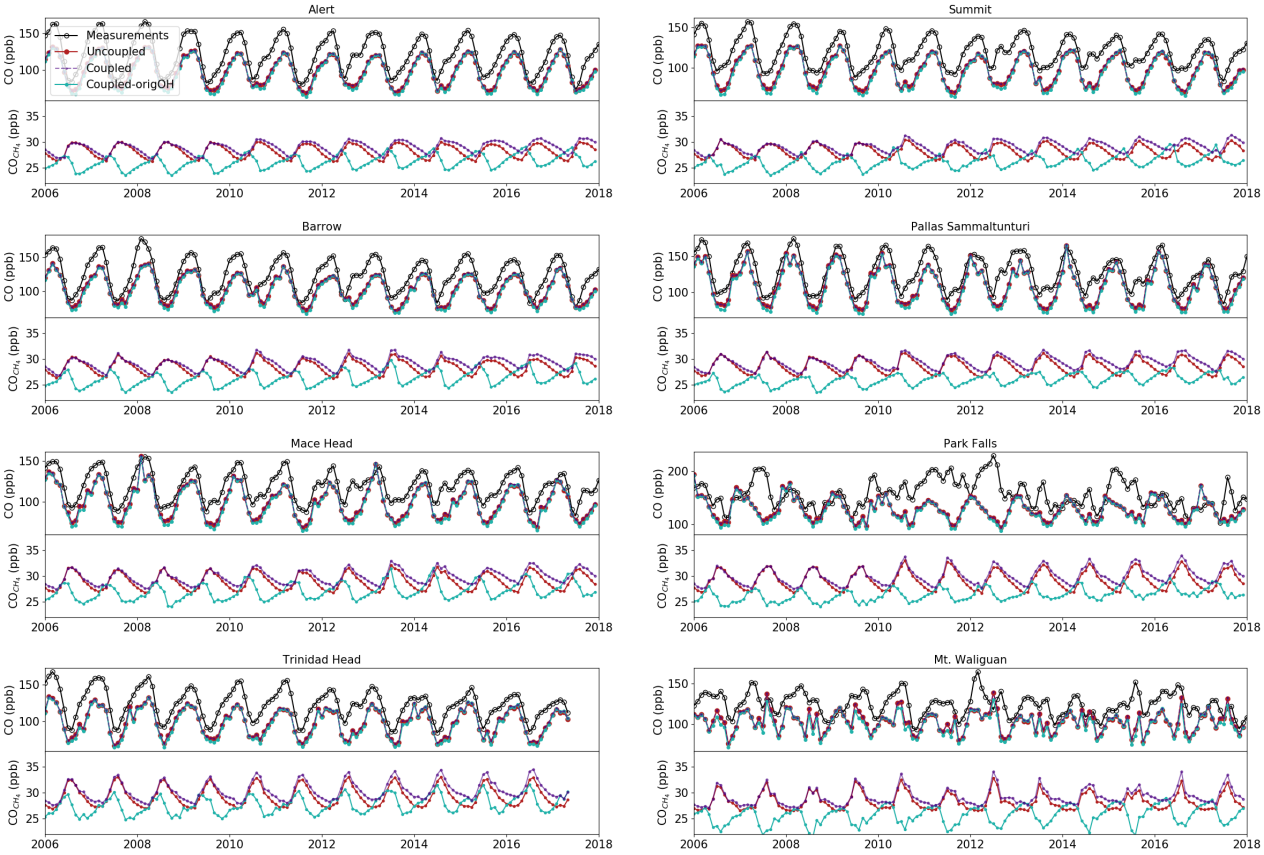

Figure S20. Modelled CO (red-uncoupled, indigo-coupled, turquoise-*coupled-origOH*) comparison with surface measurements (black, top plots), based on monthly average values. The bottom plots represent the mixing ratios of the CO production from CH_4 from the different simulations.

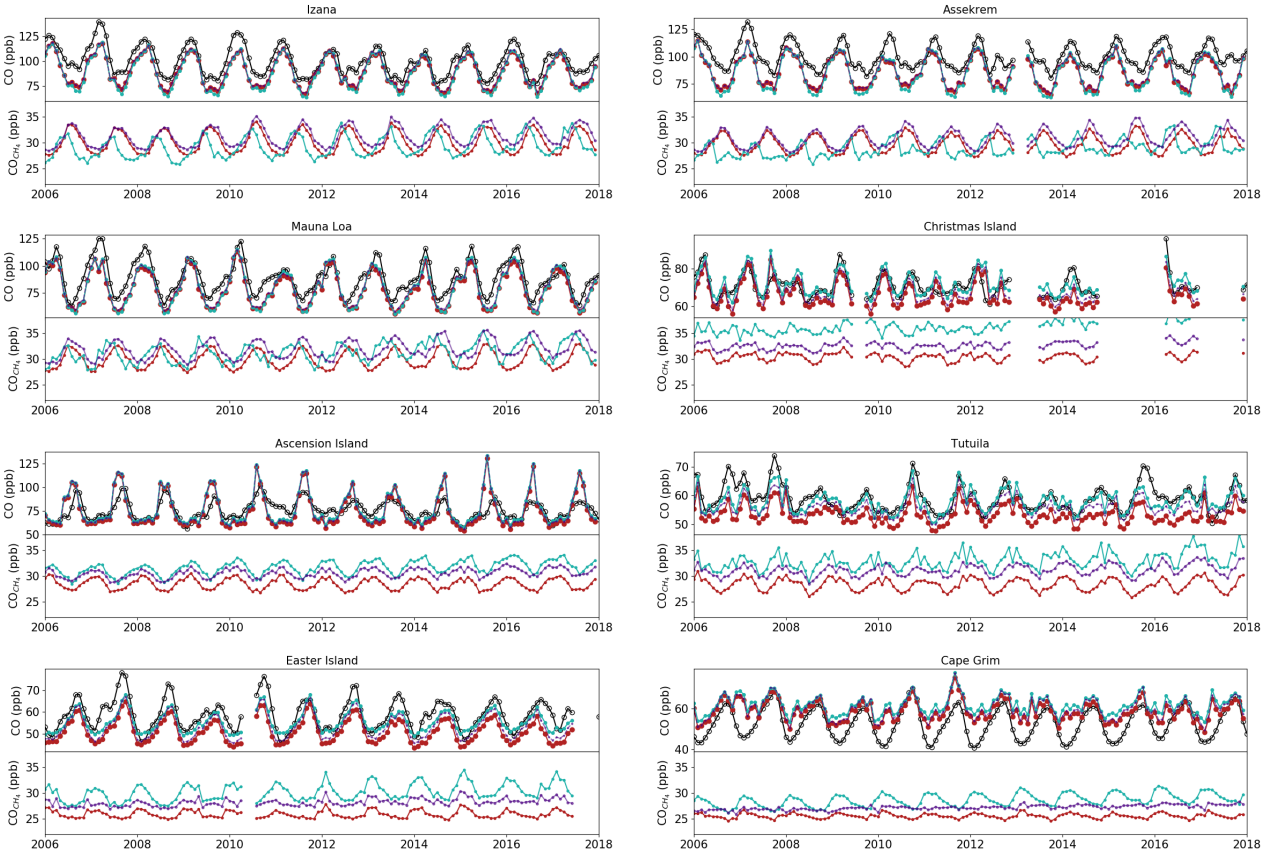

Figure S20. Continued.

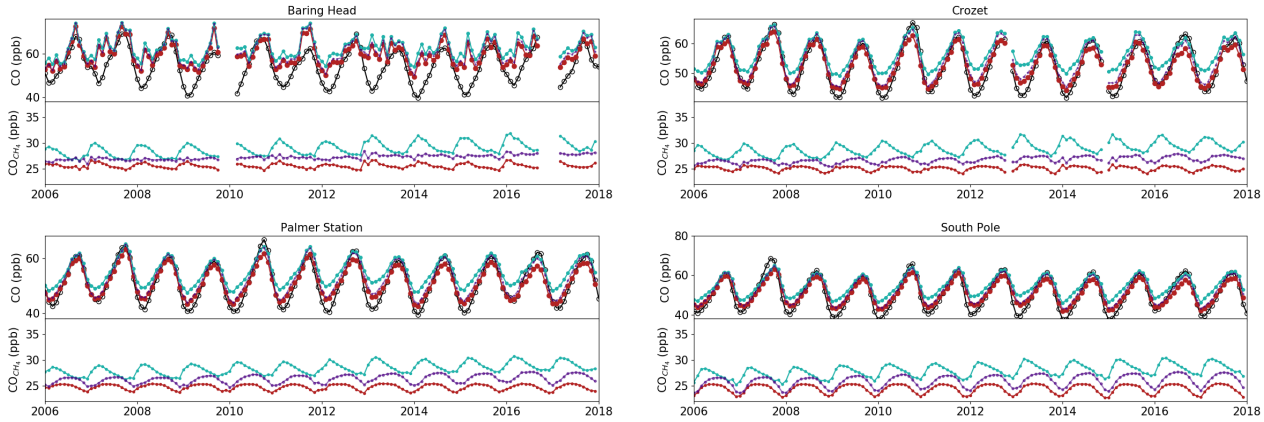

Figure S20. Continued.

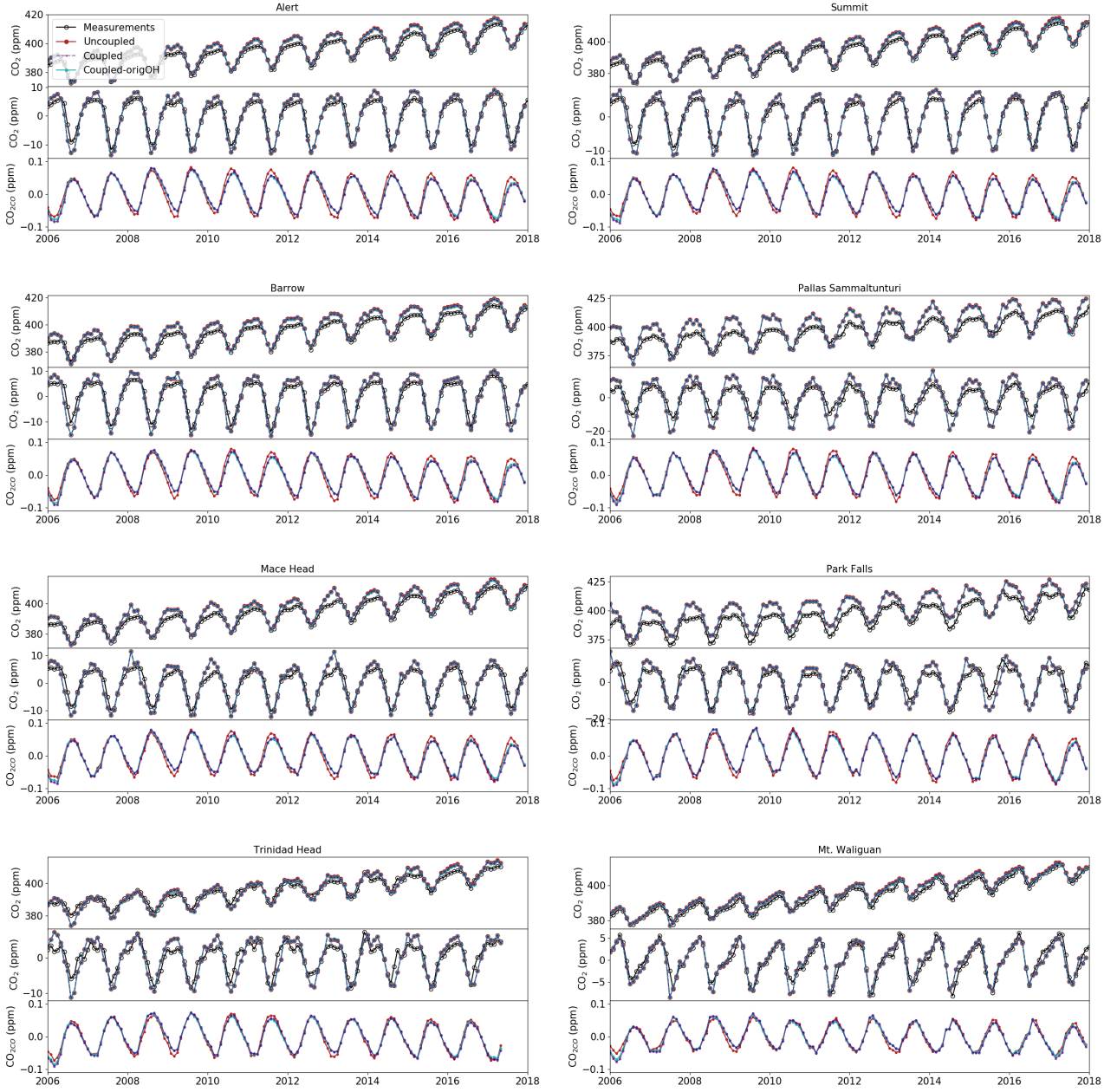

Figure S21. Modelled CO_2 (red-uncoupled, indigo-coupled, turquoise-*coupled-origOH*) comparison with surface measurements (black, top plots), based on monthly average values. The detrended values are shown in the middle plots. The bottom plots represent the detrended mixing ratios of the CO_2 production from CO from the different simulations.

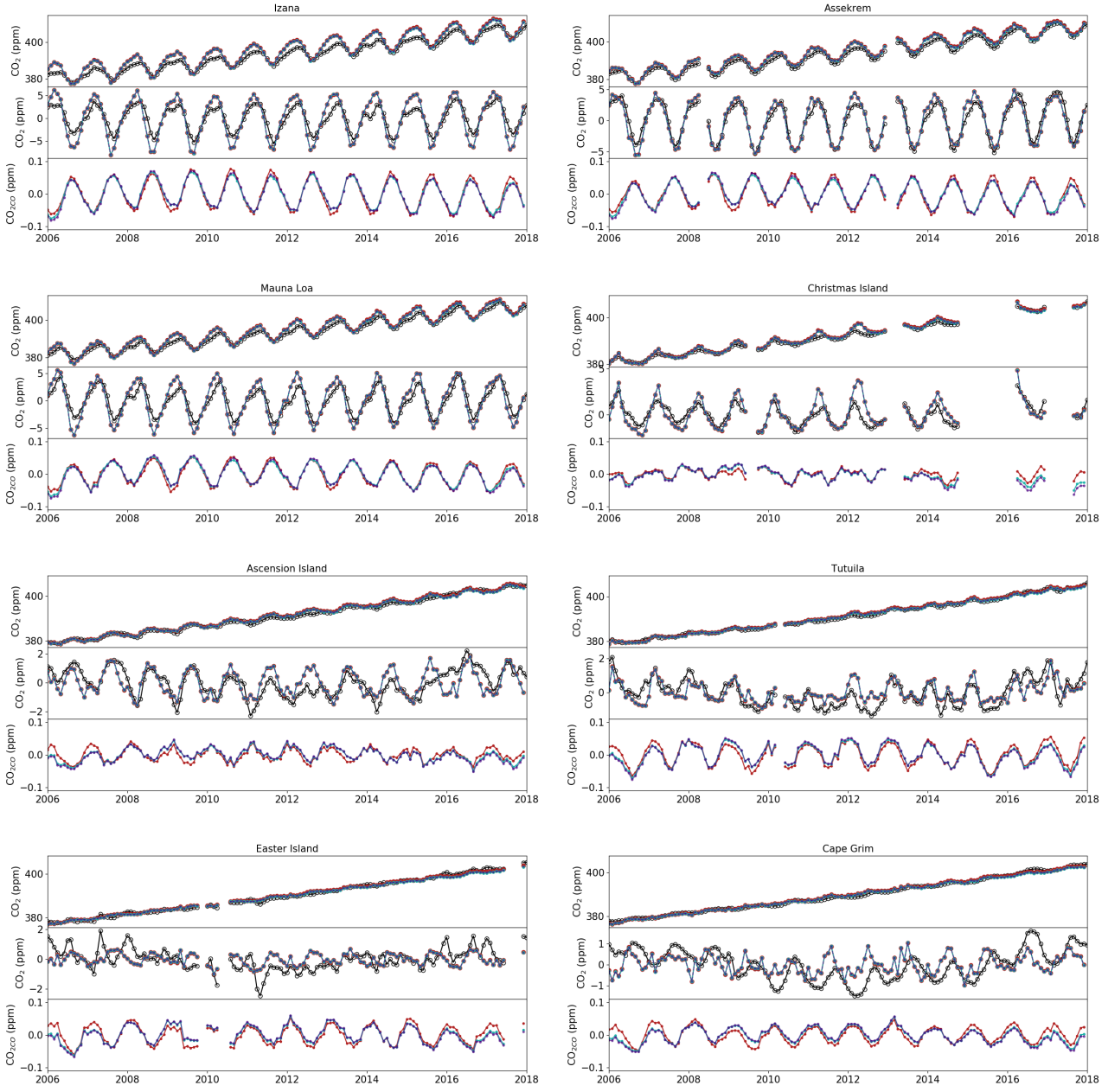

Figure S21. Continued.

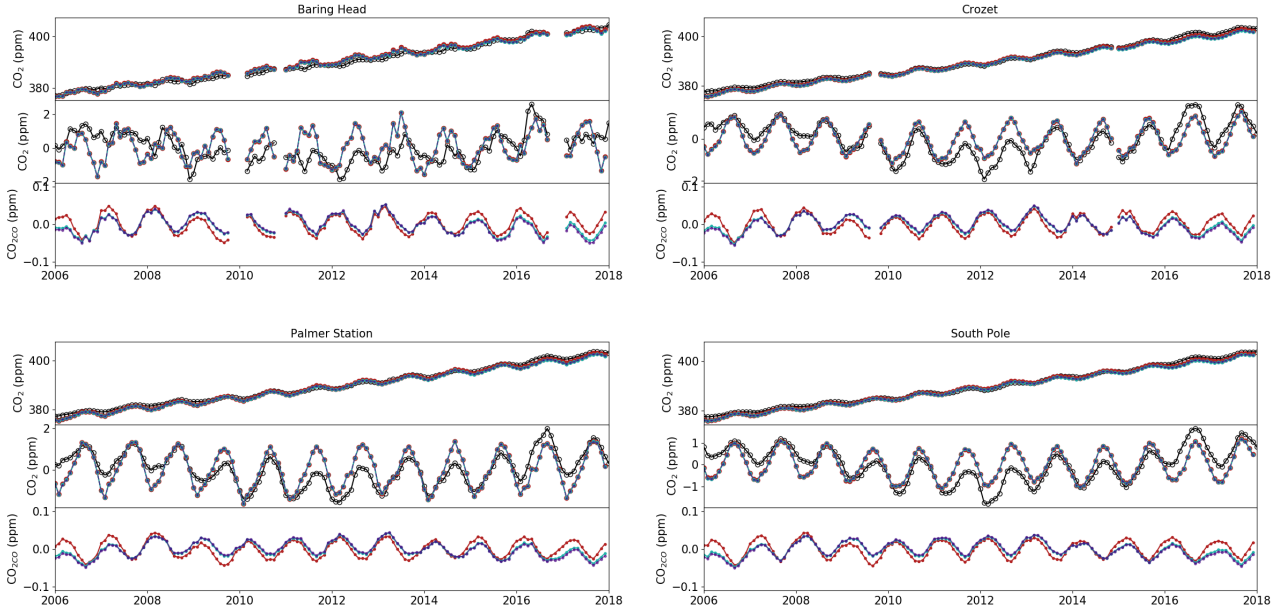

Figure S21. Continued.

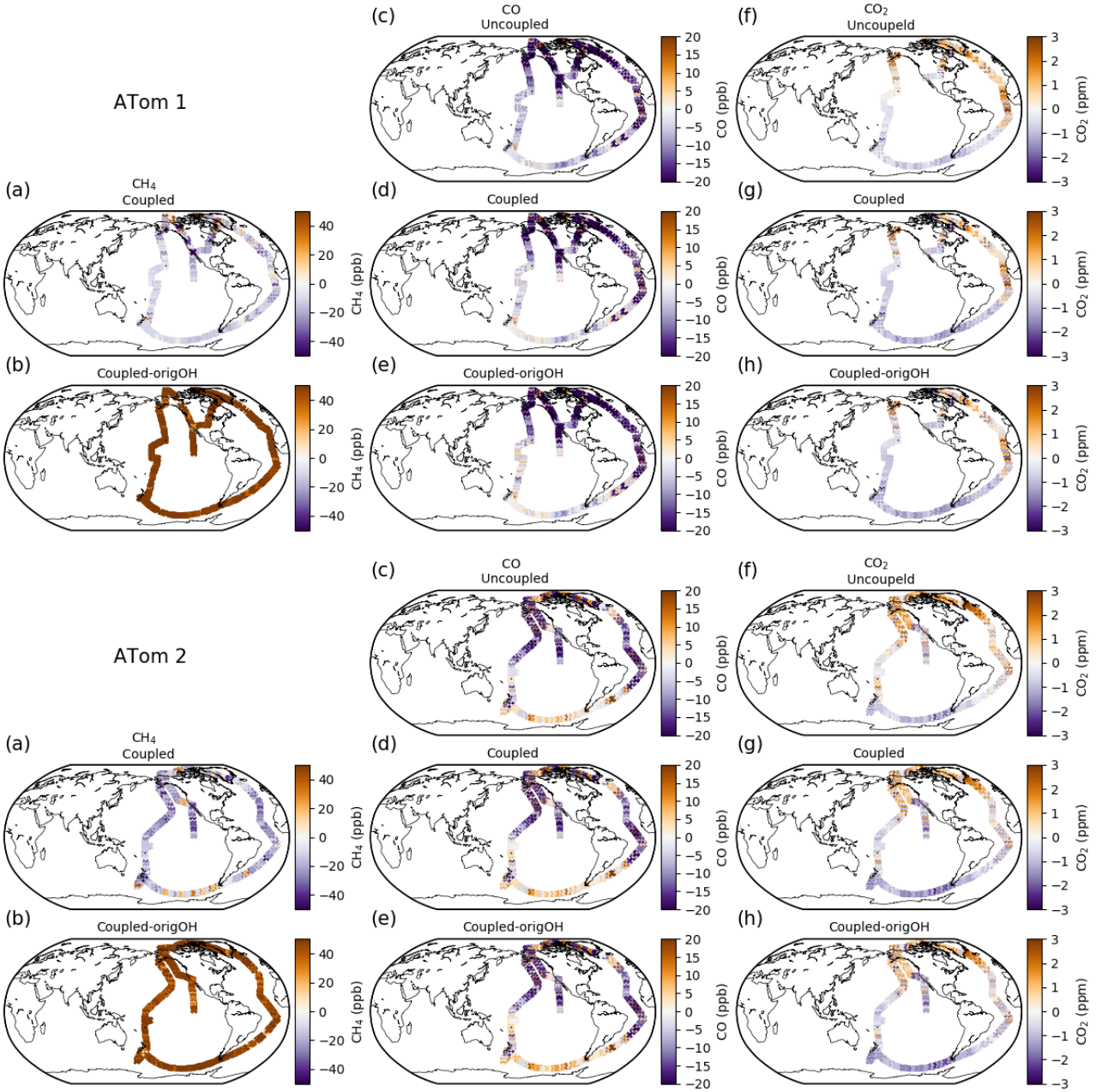

Figure S22. Model-measurement differences for CH_4 (a,b), CO (c–e) and CO_2 (f–h) based on simulated values from the uncoupled (c, f), coupled (a, d, g) and *coupled-origOH* (b, e, h) simulations during the 4 ATom campaigns.

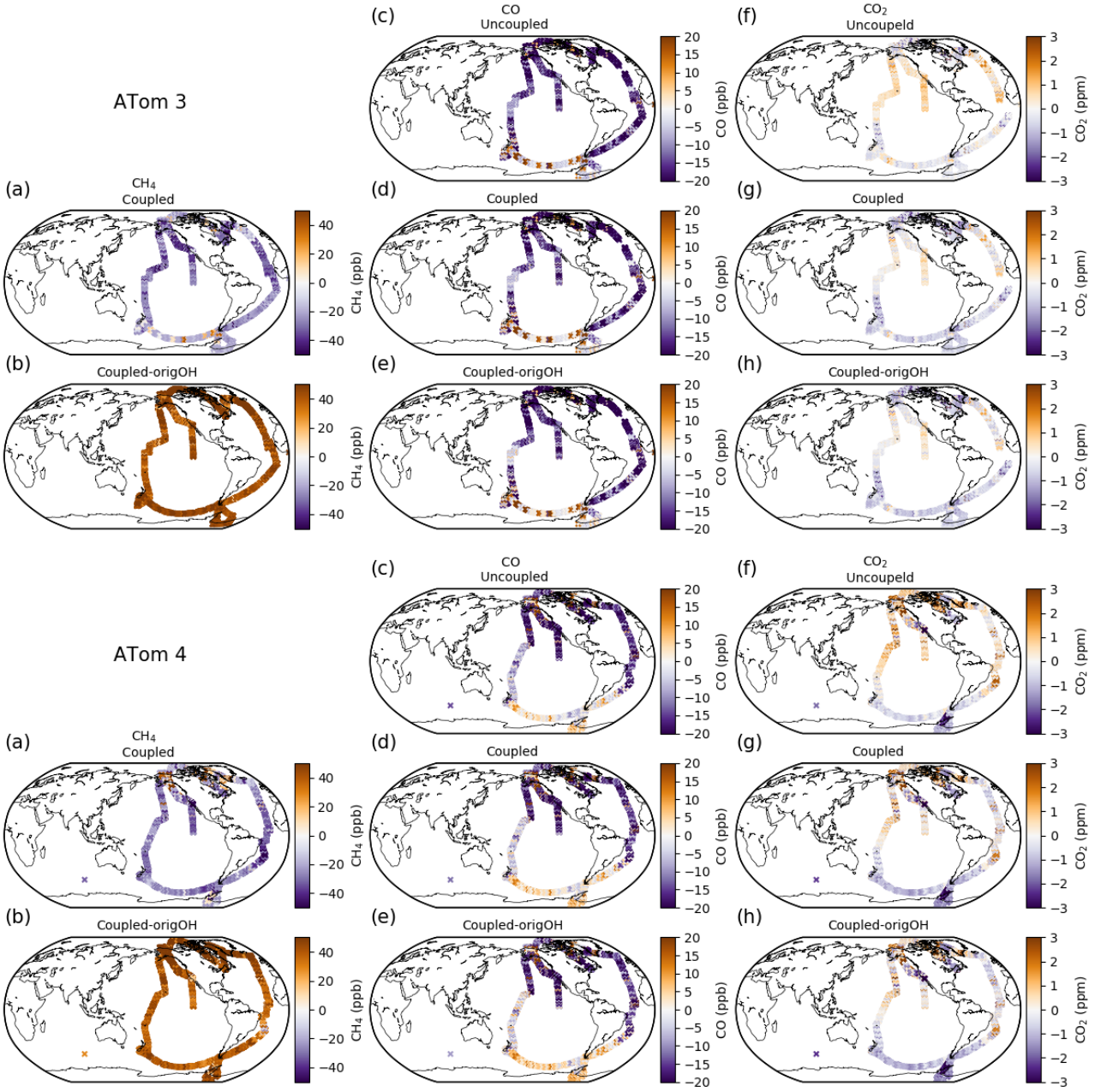

Figure S22. Continued.

References

Baker, D. F., Law, R. M., Gurney, K. R., Rayner, P., Peylin, P., Denning, A. S., Bousquet, P., Bruhwiler, L., Chen, Y.-H., Ciais, P., Fung, I. Y., Heimann, M., John, J., Maki, T., Maksyutov, S., Masarie, K., Prather, M., Pak, B., Taguchi, S., and Zhu, Z.: TransCom 3 inversion intercomparison: Impact of transport model errors on the interannual variability of regional CO_2 fluxes, 1988–2003, Global Biogeochemical Cycles, 20, https://doi.org/10.1029/2004GB002439, 2006.

Bloom, A. A., Bowman, K. W., Lee, M., Turner, A. J., Schroeder, R., Worden, J. R., Weidner, R., McDonald, K. C., and Jacob, D. J.: A global wetland methane emissions and uncertainty dataset for atmospheric chemical transport models (WetCHARTs version 1.0), Geoscientific Model Development, 10, 2141–2156, https://doi.org/10.5194/gmd-10-2141-2017, 2017.

Darmenov, A. and da Silva, A.: The quick fire emissions dataset (QFED)–documentation of versions 2.1, 2.2 and 2.4, NASA Technical Report Series on Global Modeling and Data Assimilation, NASA TM-2013-104606, 32, 183, 2015.

Fung, I., John, J., Lerner, J., Matthews, E., Prather, M., Steele, L. P., and Fraser, P. J.: Three-dimensional model synthesis of the global methane cycle, Journal of Geophysical Research: Atmospheres, 96, 13 033–13 065, https://doi.org/10.1029/91JD01247, 1991.

Kuhns, H., Knipping, E. M., and Vukovich, J. M.: Development of a United States–Mexico emissions inventory for the big bend regional aerosol and visibility observational (BRAVO) study, Journal of the Air & Waste Management Association, 55, 677–692, https://doi.org/10.1080/10473289.2005.10464648, 2005.

Lee, C., Martin, R. V., van Donkelaar, A., Lee, H., Dickerson, R. R., Hains, J. C., Krotkov, N., Richter, A., Vinnikov, K., and Schwab, J. J.: SO_2 emissions and lifetimes: Estimates from inverse modeling using in situ and global, space-based (SCIAMACHY and OMI) observations, Journal of Geophysical Research: Atmospheres, 116, https://doi.org/10.1029/2010JD014758, 2011.

Li, M., Zhang, Q., Kurokawa, J.-I., Woo, J.-H., He, K., Lu, Z., Ohara, T., Song, Y., Streets, D. G., Carmichael, G. R., Cheng, Y., Hong, C., Huo, H., Jiang, X., Kang, S., Liu, F., Su, H., and Zheng, B.: MIX: a mosaic Asian anthropogenic emission inventory under the international collaboration framework of the MICS-Asia and HTAP, Atmospheric Chemistry and Physics, 17, 935–963, https://doi.org/10.5194/acp-17-935-2017, 2017.

Maasakkers, J. D., Jacob, D. J., Sulprizio, M. P., Turner, A. J., Weitz, M., Wirth, T., Hight, C., DeFigueiredo, M., Desai, M., Schmeltz, R., Hockstad, L., Bloom, A. A., Bowman, K. W., Jeong, S., and Fischer, M. L.: Gridded national inventory of US methane emissions, Environmental science & technology, 50, 13 123–13 133, https://doi.org/10.1021/acs.est.6b02878, 2016.

Maasakkers, J. D., Jacob, D. J., Sulprizio, M. P., Scarpelli, T. R., Nesser, H., Sheng, J.-X., Zhang, Y., Hersher, M., Bloom, A. A., Bowman, K. W., Worden, J. R., Janssens-Maenhout, G., and Parker, R. J.: Global distribution of methane emissions, emission trends, and OH concentrations and trends inferred from an inversion of GOSAT satellite data for 2010–2015, Atmospheric Chemistry and Physics, 19, 7859–7881, https://doi.org/10.5194/acp-19-7859-2019, 2019.

Messerschmidt, J., Parazoo, N., Wunch, D., Deutscher, N. M., Roehl, C., Warneke, T., and Wennberg, P. O.: Evaluation of seasonal atmosphere–biosphere exchange estimations with TCCON measurements, Atmospheric Chemistry and Physics, 13, 5103–5115, https://doi.org/10.5194/acp-13-5103-2013, 2013.

Oda, T. and Maksyutov, S.: A very high-resolution (1 km×1 km) global fossil fuel CO_2 emission inventory derived using a point source database and satellite observations of nighttime lights, Atmospheric Chemistry and Physics, 11, 543–556, https://doi.org/10.5194/acp-11-543-2011, 2011.

Sheng, J.-X., Jacob, D. J., Maasakkers, J. D., Sulprizio, M. P., Zavala-Araiza, D., and Hamburg, S. P.: A high-resolution (0.1° × 0.1°) inventory of methane emissions from Canadian and Mexican oil and gas systems, Atmospheric Environment, 158, 211–215, https://doi.org/10.1016/j.atmosenv.2017.02.036, 2017.

Stettler, M., Eastham, S., and Barrett, S.: Air quality and public health impacts of UK airports. Part I: Emissions, Atmospheric Environment, 45, 5415–5424, https://doi.org/10.1016/j.atmosenv.2011.07.012, 2011.

Takahashi, T., Sutherland, S. C., Wanninkhof, R., Sweeney, C., Feely, R. A., Chipman, D. W., Hales, B., Friederich, G., Chavez, F., Sabine, C., et al.: Climatological mean and decadal change in surface ocean pCO_2, and net sea–air CO_2 flux over the global oceans, Deep Sea Research Part II: Topical Studies in Oceanography, 56, 554–577, 2009.

Van Donkelaar, A., Martin, R. V., Pasch, A. N., Szykman, J. J., Zhang, L., Wang, Y. X., and Chen, D.: Improving the accuracy of daily satellite-derived ground-level fine aerosol concentration estimates for North America, Environmental science & technology, 46, 11 971–11 978, https://doi.org/doi.org/10.1021/es3025319, 2012.

Vestreng, V., Mareckova, K., Kakareka, S., Malchykhina, A., and Kukharchyk, T.: Inventory Review 2007. Stage 1 and 2 review. Emission data reported to LRTAP Convention and NEC Directive, review of gridded data and review of PM inventories in Belarus, Republic of Moldova, Russian Federation and Ukraine, 2007.

Yevich, R. and Logan, J. A.: An assessment of biofuel use and burning of agricultural waste in the developing world, Global Biogeochemical Cycles, 17, https://doi.org/10.1029/2002GB001952, 2003.